10.1071/CH19117_AC

Australian Journal of Chemistry 2019, 72(9), 674-692

Supplementary Material

Pd (II) immobilized on ferromagnetic multi-walled carbon nanotubes functionalized by aminated 2-chloroethylphosphonic acid with *S*-methylisothiourea (FMMWCNTs@CPA@SMTU@Pd^{II} NPs) applied as a highly efficient and recyclable nanostructured catalyst for Suzuki-Miyaura and Mizoroki-Heck cross-coupling reactions in solvent-free conditions

Maryam Sadat Ghasemzadeh[A] *and Batool Akhlaghinia*[A,B]

[A]Department of Chemistry, Faculty of Science, Ferdowsi University of Mashhad, Mashhad 9177948974, Iran.

[B]Corresponding author. Email: akhlaghinia@um.ac.ir

Experimental

Materials and Instruments

All chemical reagents and solvents were purchased from Merck and Sigma-Aldrich chemical companies and were used as received without further purification. The purity determinations of the products were accomplished by TLC on silica gel polygram STL G/UV 254 plates. The melting points of the products were determined with an Electrothermal Type 9100 melting point apparatus. The FT-IR spectra were recorded on an Avatar 370 FT-IR Therma Nicolet spectrometer. Elemental analyses were performed using a Thermo Finnegan Flash EA 1112 Series instrument. The NMR spectra were obtained in Brucker Avance 300 and 400 MHz instruments in $CDCl_3$. Mass spectra were recorded with a CH7A Varianmat Bremem instrument at 70 eV electron impact ionization, in m/z (rel %). The crystal structure of catalyst was analyzed by XRD using Model Explorer Company: GNR (Italy) diffractometer Dectvis operated at 40 kV and 30 mA utilizing Cu Kα radiation (λ= 0.154 Aº). Transmission electron microscopy (TEM) was performed with a Leo 912 AB microscope (Zeiss, Germany) with an accelerating voltage of 120 kV. FE-SEM images, EDS and EDS-map were recorded using a TESCAN, Model: MIRA3 scanning electron microscope operating at an acceleration voltage of 30.0 kV and resolution of about 200 and 500 nm (manufactured in the Czech Republic). TGA analysis was carried out on a Shimadzu Thermogravimetric Analyzer (TG-50) in the temperature range of 25-920 ºC at a heating rate of 10 ºC min^{-1} under air atmosphere. The magnetic properties of the catalyst were measured using a vibrating sample magnetometer (VSM, Magnetic Danesh Pajoh Inst.). X-ray photoelectron spectroscopy (XPS) were performed using the Thermo Scientifi, ESCALAB 250 Xi Mg X-ray resource and Bestec Al X-ray Kα: 1486.6 (manufactured in Germany). UV-Vis diffuse reflectance spectroscopy (DRS) was measured using an Ava Spec 2048 TECH spectrometer. Inductively coupled plasma atomic emission spectroscopy (ICP-OES) was carried out with a Varian VISTA-PRO, CCD (Australia). All yields refer to isolated products after purification by thin layer chromatography and/or column chromatography.

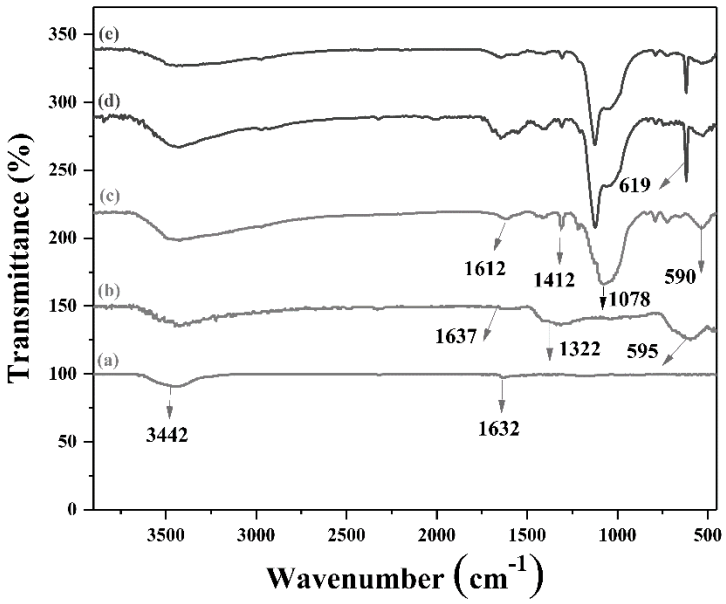

Fig. S1. FT-IR spectra of (a) MWCNTs, (b) FMMWCNTs (**I**), (c) FMMWCNTs@CPA (**II**), (d) FMMWCNTs@CPA@SMTU (**III**) and (e) FMMWCNTs@CPA@SMTU@Pd^{II} NPs (**IV**).

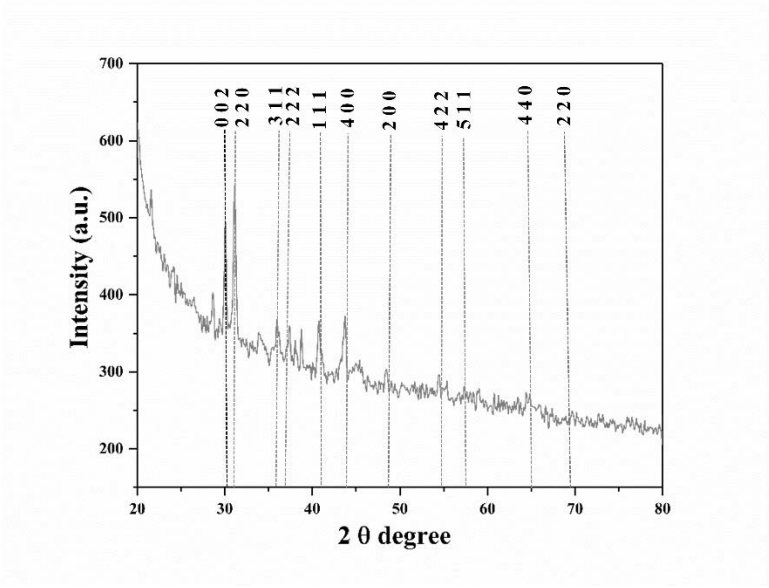

Fig. S2. XRD pattern of FMMWCNTs@CPA@SMTU@Pd^{II} NPs (**IV**).

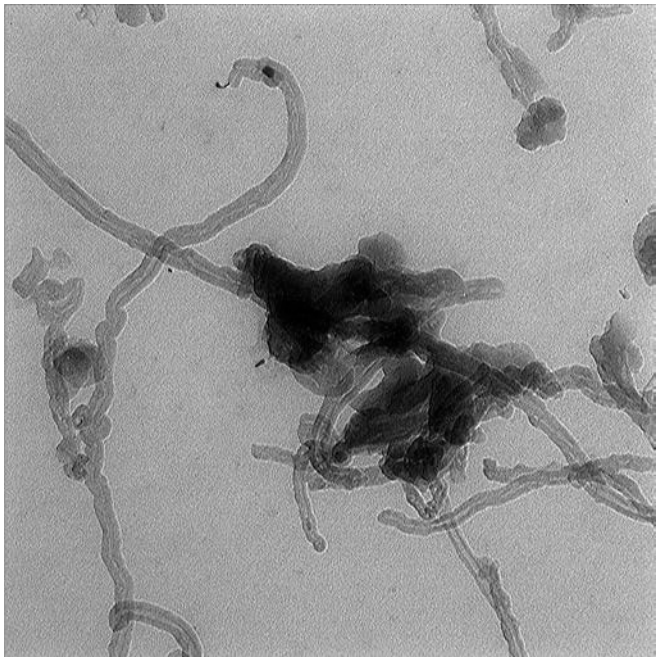

Fig. S3. TEM image of FMMWCNTs@CPA@SMTU@Pd^{II} NPs (**IV**).

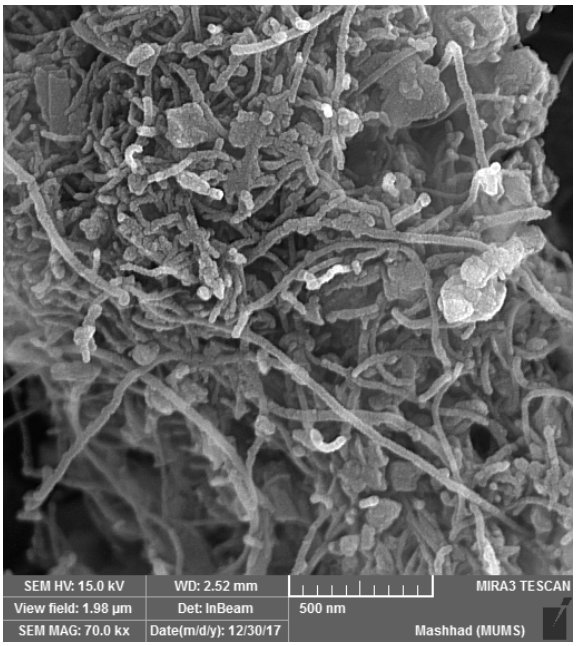

Fig. S4. The FE-SEM image of FMMWCNTs@CPA@SMTU@Pd^{II} NPs (**IV**).

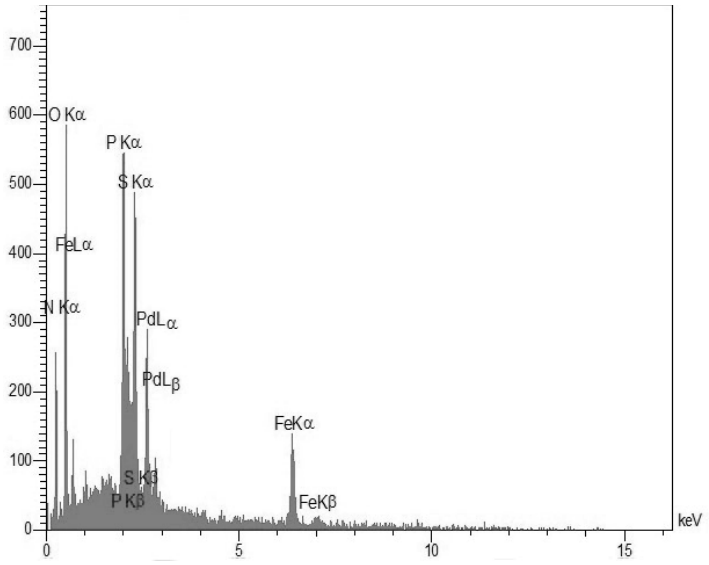

Fig. S5. The EDS analysis of FMMWCNTs@CPA@SMTU@Pd^{II} NPs (**IV**).

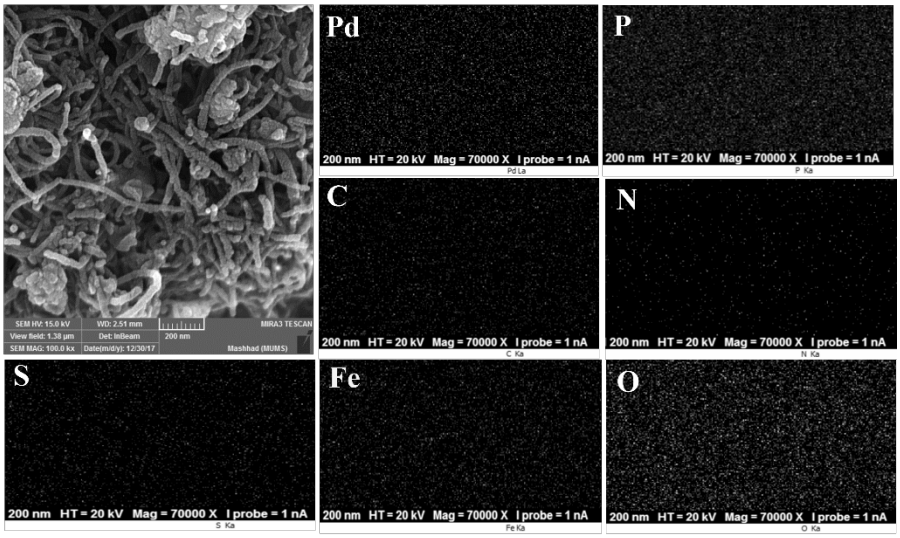

Fig. S6. EDS-map images of FMMWCNTs@CPA@SMTU@Pd^{II} NPs (**IV**).

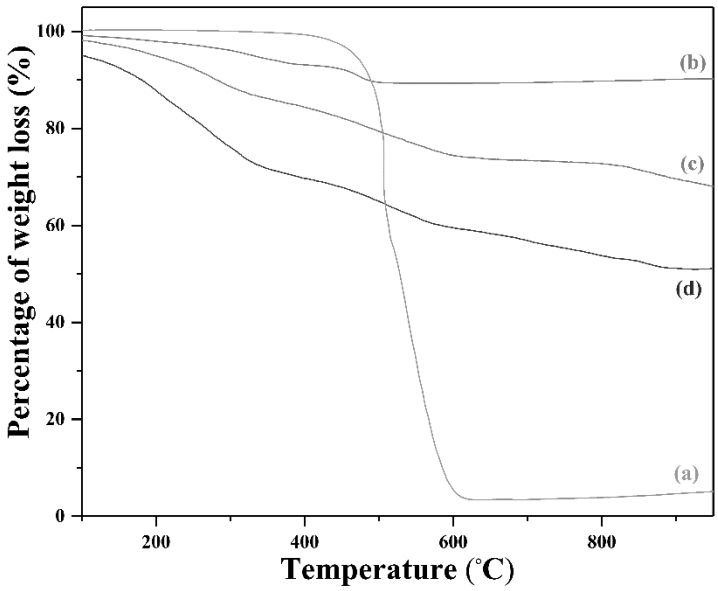

Fig. S7. TGA thermograms of (a) MWCNTs, (b) FMMWCNTs@CPA (**II**), (c) FMMWCNTs@CPA@SMTU (**III**) and (d) FMMWCNTs@CPA@SMTU@Pd^{II} NPs (**IV**).

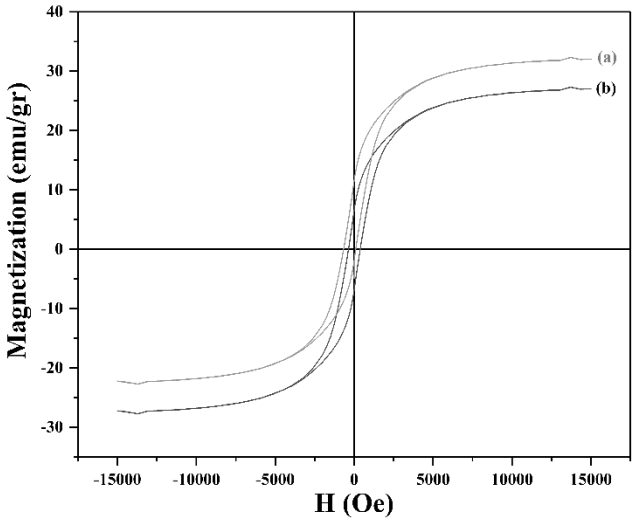

Fig. S8. Magnetization curves of (a) FMMWCNTs (**I**) and (b) FMMWCNTs@CPA@SMTU@Pd^{II} NPs (**IV**).

Table S1. Magnetic properties of MMWCNTs (**I**) and MMWCNTs@CPA@SMTU@Pd^{II} NPs (**IV**).

Sample	Saturation magnetization (M_s), emu/g	Coercivity (H_{ci}), Oe	Remnant magnetization (M_r), emu/g
FMMWCNTs (**I**)	[31.98]	[560]	[14.04]
FMMWCNTs@CPA@SMTU@Pd^{II} NPs (**IV**)	[26.95]	[440]	[11.60]

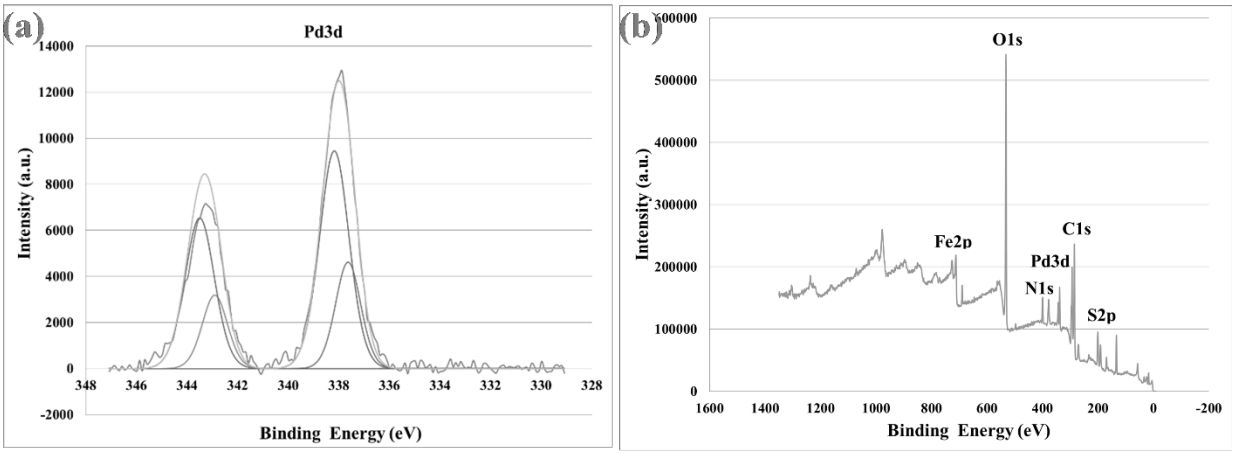

Fig. S9. XPS spectrum of (a) FMMWCNTs@CPA@SMTU@Pd^{II} NPs (**IV**) showing Pd $3d_{5/2}$ and Pd $3d_{3/2}$ binding energies and (b) XPS elemental survey scan of nanostructured catalyst.

1, 1'-Biphenyl (**1a**) (0.279 g, 98 %): white solid; mp 70-71 ºC (Lit.[1, 15] 70-72 ºC). δ_H (400 MHz, $CDCl_3$) 7.54 (d, *J* 8, 4H), 7.39 (t, *J* 8, 4H), 7.31-7.27 (m, 2H). δ_C (125 MHz, $CDCl_3$) 141.2, 128.7, 127.2, 126.1. *m/z* 154 (M^+, 80 %), 153 (M-1H, 102), 115 (M-C_3H_3, 32), 102 (M-C_4H_4, 28), 76 (M-C_6H_6, 78).

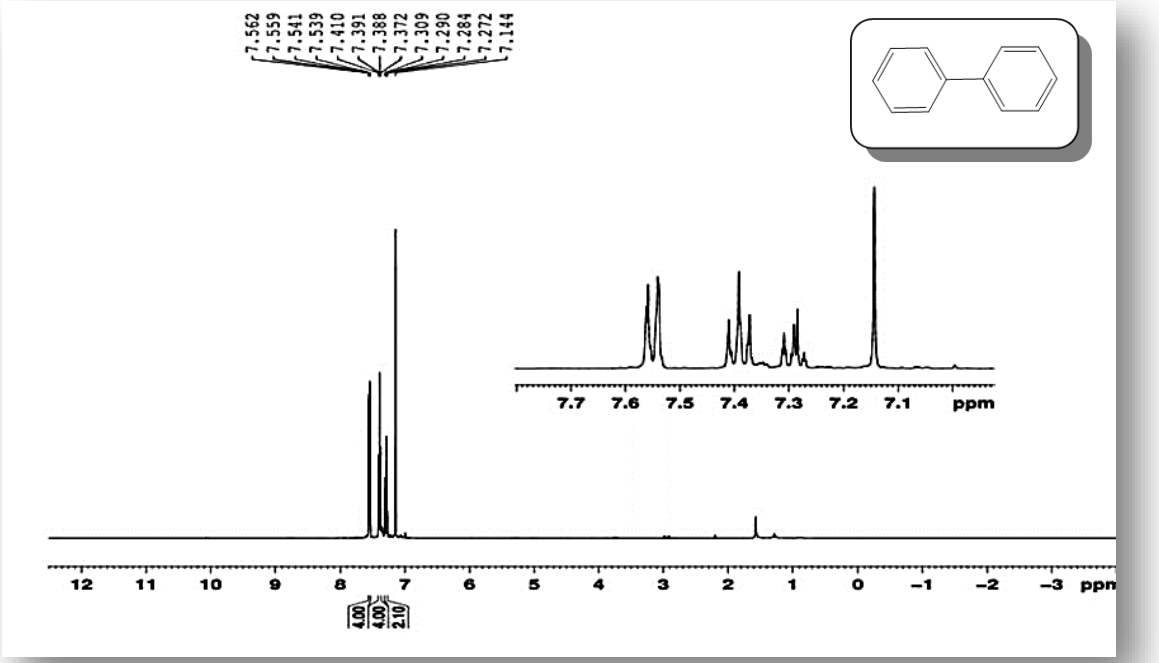

Fig. S10. ^1H NMR (400 MHz, $CDCl_3$) of 1, 1'-Biphenyl (1a).

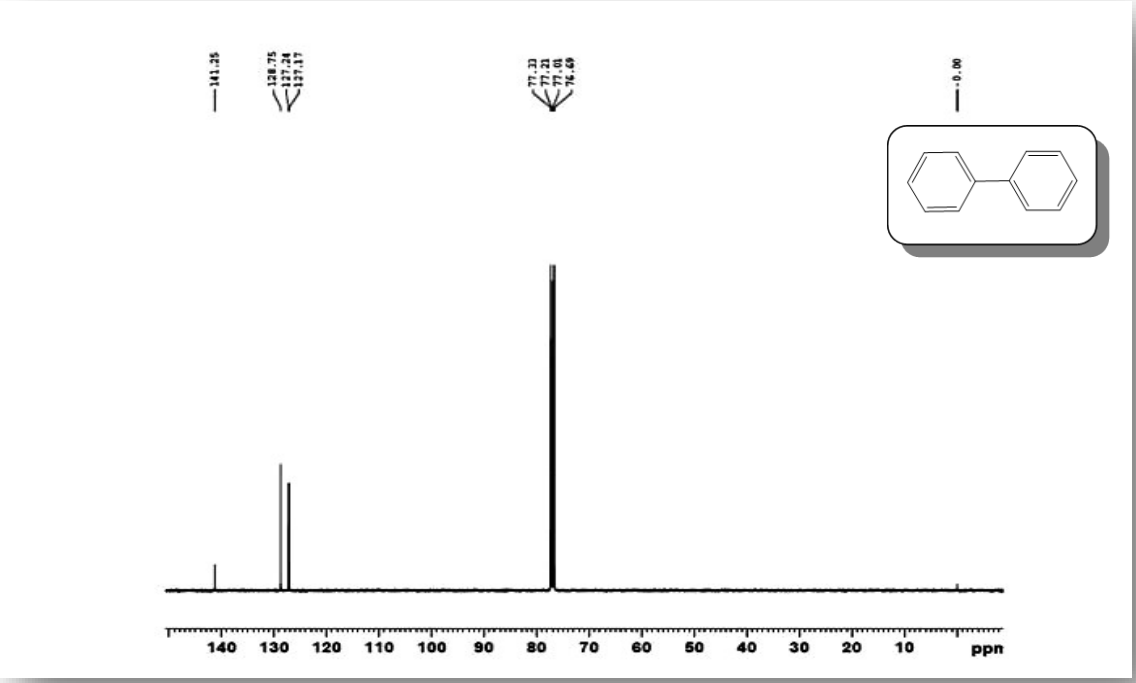

Fig. S11. ^{13}C NMR (125 MHz, $CDCl_3$) of 1, 1'-Biphenyl (1a).

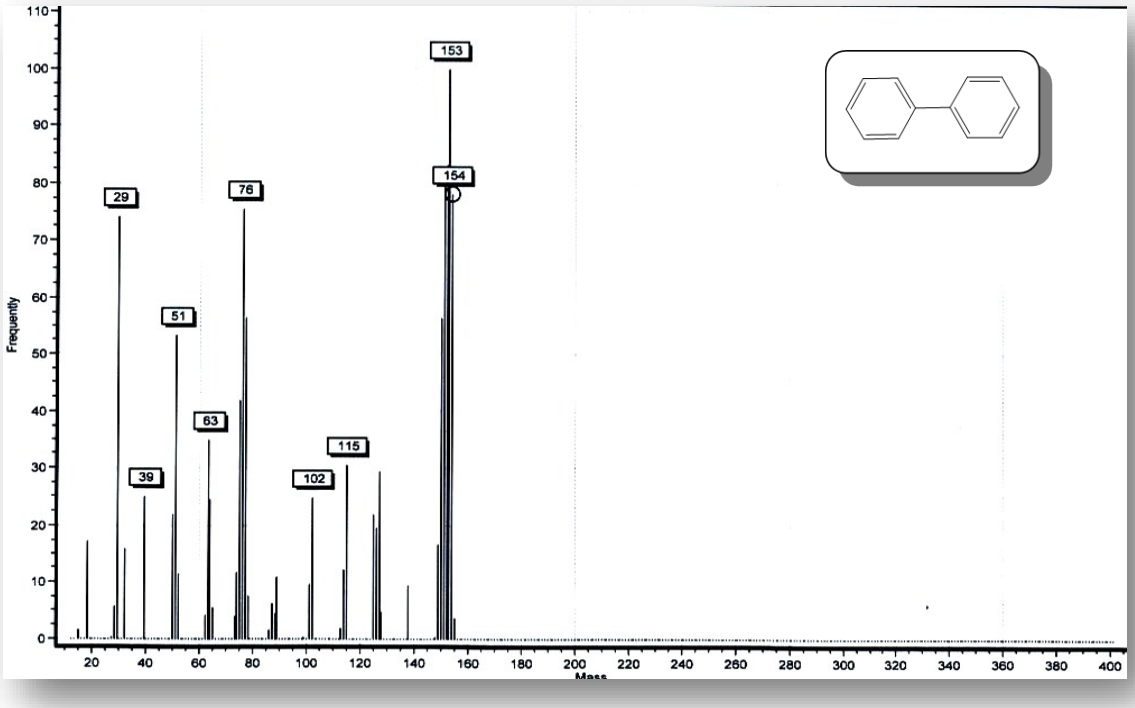

Fig. S12. Mass spectrum of 1, 1'-Biphenyl (1a).

4-Methoxy-1, 1'-biphenyl (**1c**) (0.265 g, 90%): white solid; mp 88-90 ºC (Lit.[2, 10, 15] 87-90 ºC). δ_H (400 MHz, $CDCl_3$) 7.45 (t, *J* 8.4, 4H), 7.34 (t, *J* 7.6, 2H), 7.21 (t, *J* 6.8, 1H), 6.89 (d, *J* 8.8, 2H), 3.75 (s, 3H). δ_C (125 MHz, $CDCl_3$) 159.1, 140.8, 133.8, 128.7, 128.1, 126.7, 114.2, 55.3. *m/z* 184 (M^+, 80%), 183 (M-1H, 102), 168 (M-CH_3, 84), 152 (M-CH_4O, 42), 140 (M-C_3H_8, 82), 115 (M-C_4H_5O, 80), 92 (M-C_6H_5O, 44).

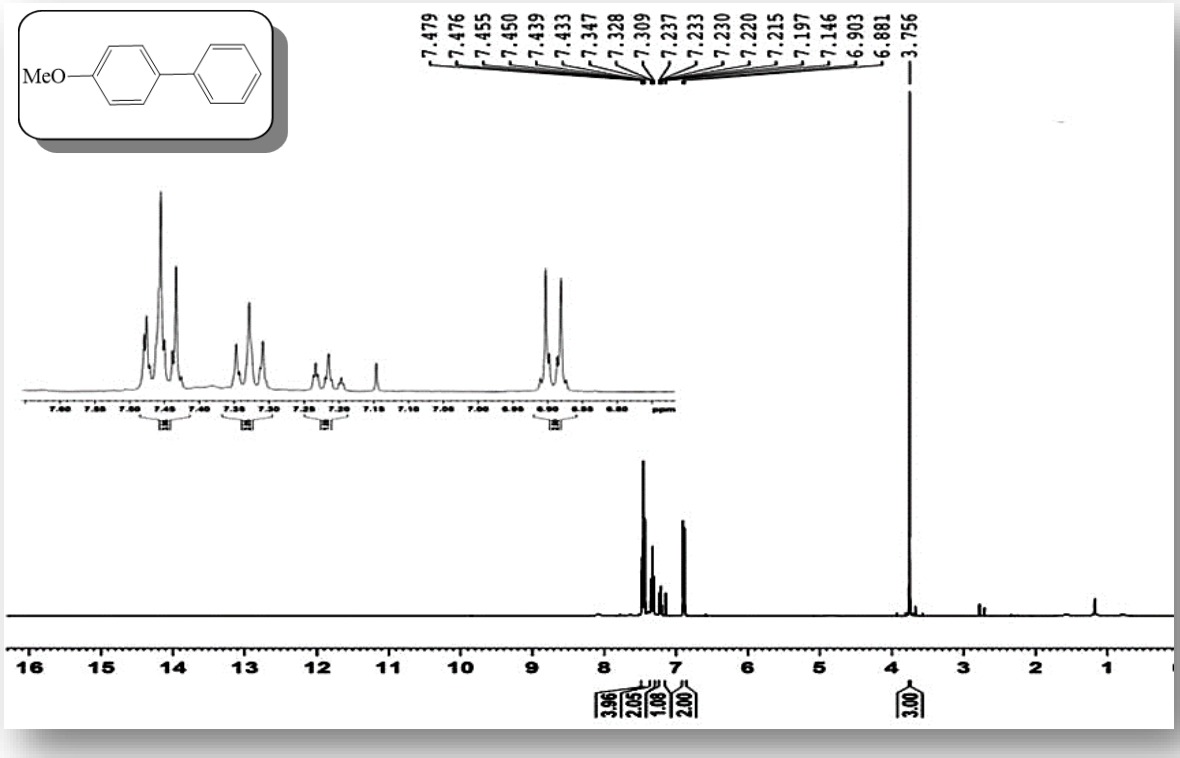

Fig. S13. ^1H NMR (400 MHz, $CDCl_3$) of 4-Methoxy-1, 1'-biphenyl (1c).

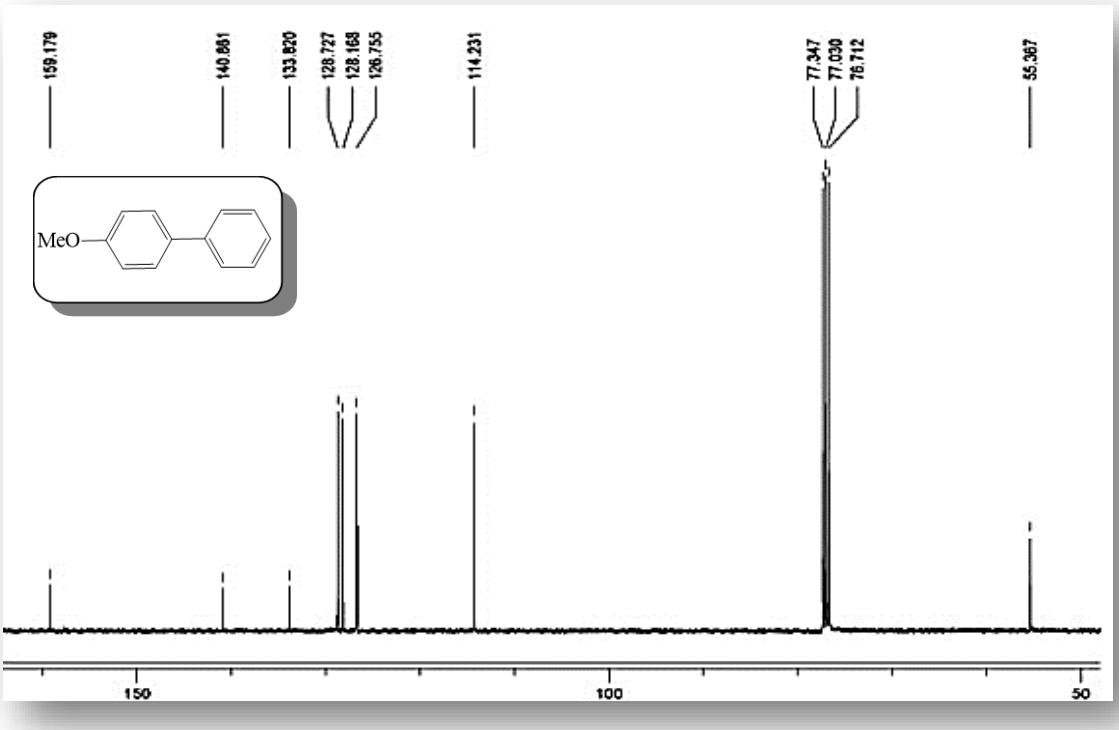

Fig. S14. ^{13}C NMR (125 MHz, $CDCl_3$) of 4-Methoxy-1, 1'-biphenyl (1c).

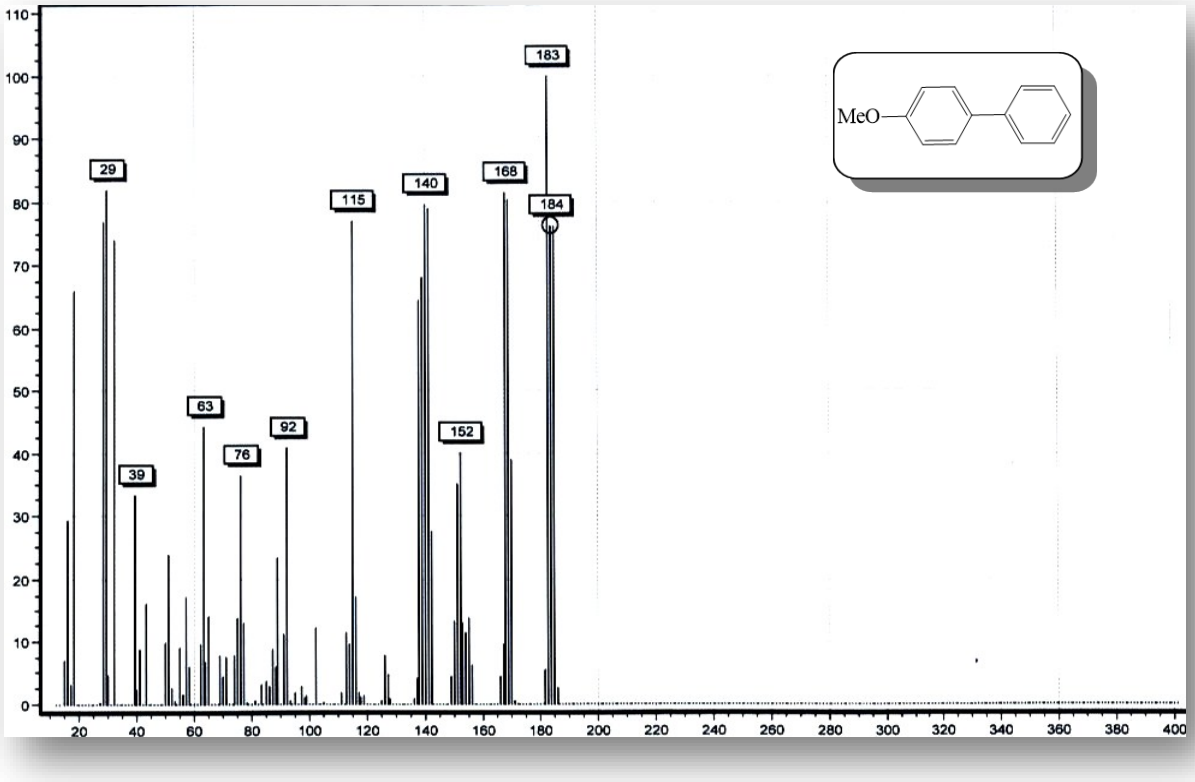

Fig. S15. Mass spectrum of 4-Methoxy-1, 1'-biphenyl (1c).

(*E*)-Butyl cinnamate (**1f**) (0.229 g, 95%): white solid; mp 141-142 ºC (Lit.[3, 11, 12, 14, 15] 140-142 ºC). δ_H (400 MHz, $CDCl_3$) 7.60 (d, *J* 16.4, 1H), 7.45-7.43 (m, 1H), 7.31-7.28 (m, 1H), 6.38 (d, *J* 16, 1H), 6.34 (d, *J* 16, 1H), 4.13 (t, *J* 6.8, 2H), 1.62-1.59 (m, 2H), 1.36-1.34 (m, 2H), 0.88 (t, *J* 7.6, 3H). δ_C (100 MHz, $CDCl_3$) 166.8, 144.4, 134.4, 130.1, 128.8, 128.0, 118.2, 64.3, 30.8, 19.2, 13.7.

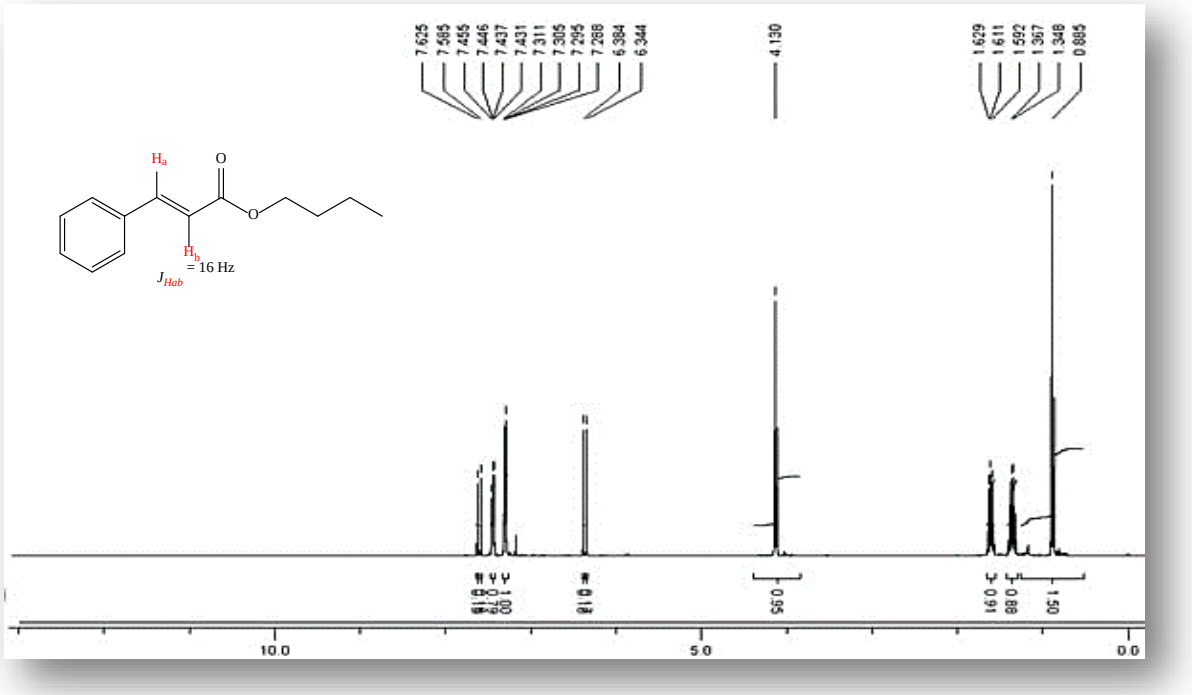

Fig. S16. ^{1}H NMR (400 MHz, $CDCl_3$) of (*E*)-Butyl cinnamate (1f).

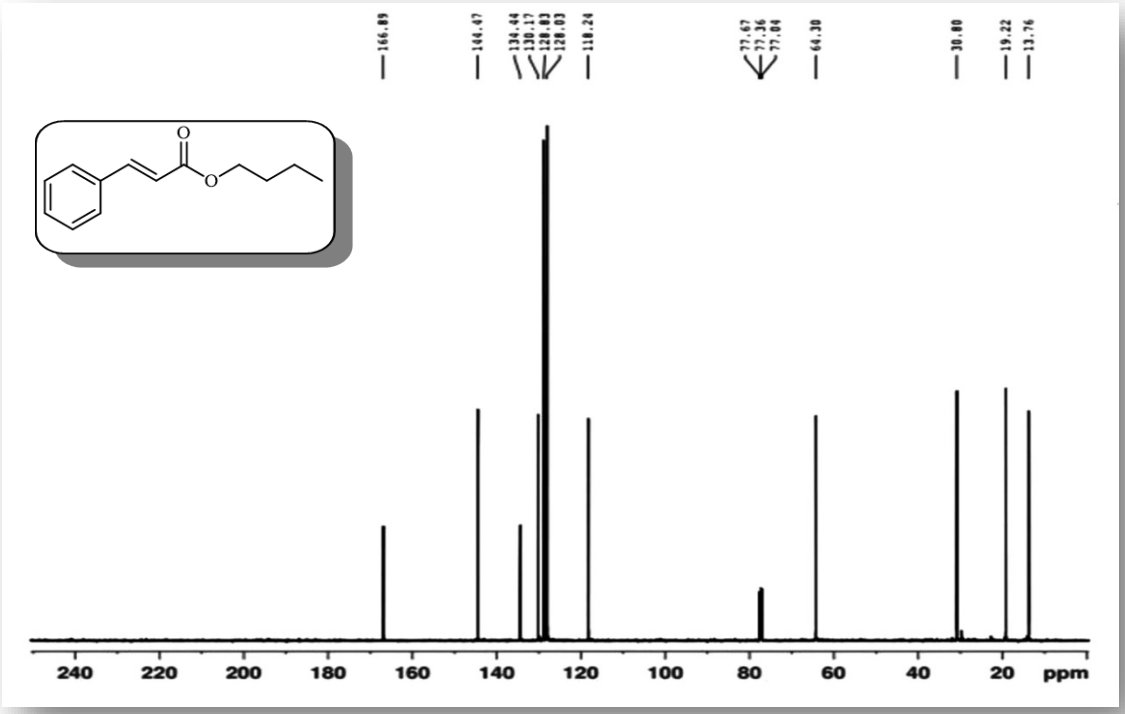

Fig. S17. ^{13}C NMR (100 MHz, $CDCl_3$) of (*E*)-Butyl cinnamate (1f).

(*E*)-Methyl 3-(4-nitrophenyl) acrylate (**2d**) (0.277 g, 95%): white solid; mp 161-162 ºC (Lit.[4, 13, 15] 160-162 ºC). δ_H (300 MHz, $CDCl_3$) 8.25 (d, *J* 8.8, 2H), 7.72 (d, *J* 16.1, 1H), 7.67 (d, *J* 8.7, 2H), 6.56 (d, *J* 16.1, 1H), 3.84 (s, 3H). δ_C (75 MHz, $CDCl_3$) 166.6, 148.7, 142.1, 140.7, 128.8, 124.4, 122.3, 52.3. *m/z* 207 (M^+, 62 %), 206 (M-1H, 92), 189 (M-C_2H_6O, 38), 175 (M-CH_4O, 102), 148 (M-$C_2H_3O_2$, 52), 129 (M-$C_3H_{10}O_4$, 80), 118 (M-$C_4H_9O_2$, 78), 102 (M-$C_6H_1O_2$, 88).

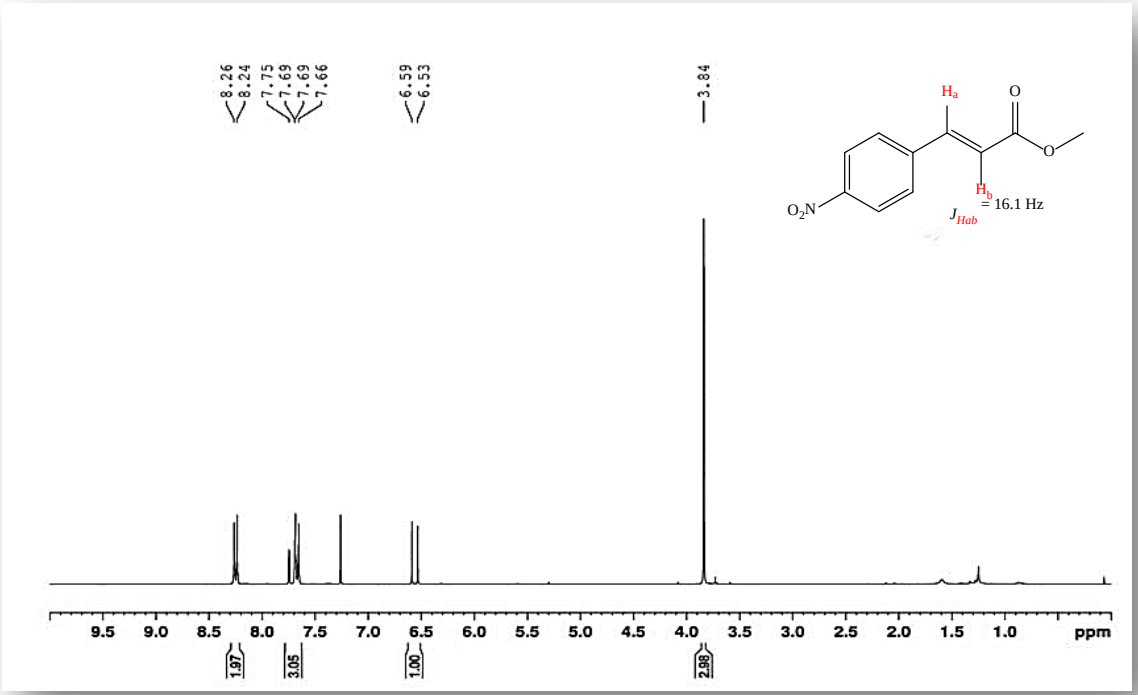

Fig. S18. ^{1}H NMR (300 MHz, $CDCl_3$) of (*E*)-Methyl 3-(4-nitrophenyl) acrylate (2d).

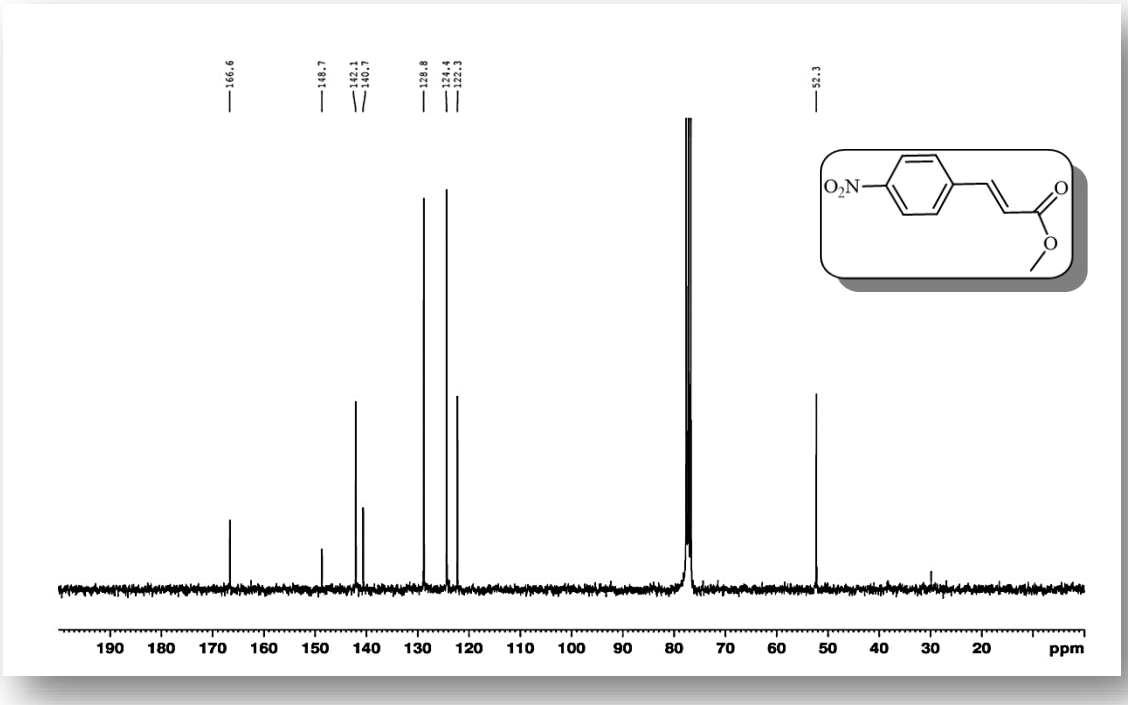

Fig. S19. ^{13}C NMR (75 MHz, $CDCl_3$) of (*E*)-Methyl 3-(4-nitrophenyl) acrylate (2d).

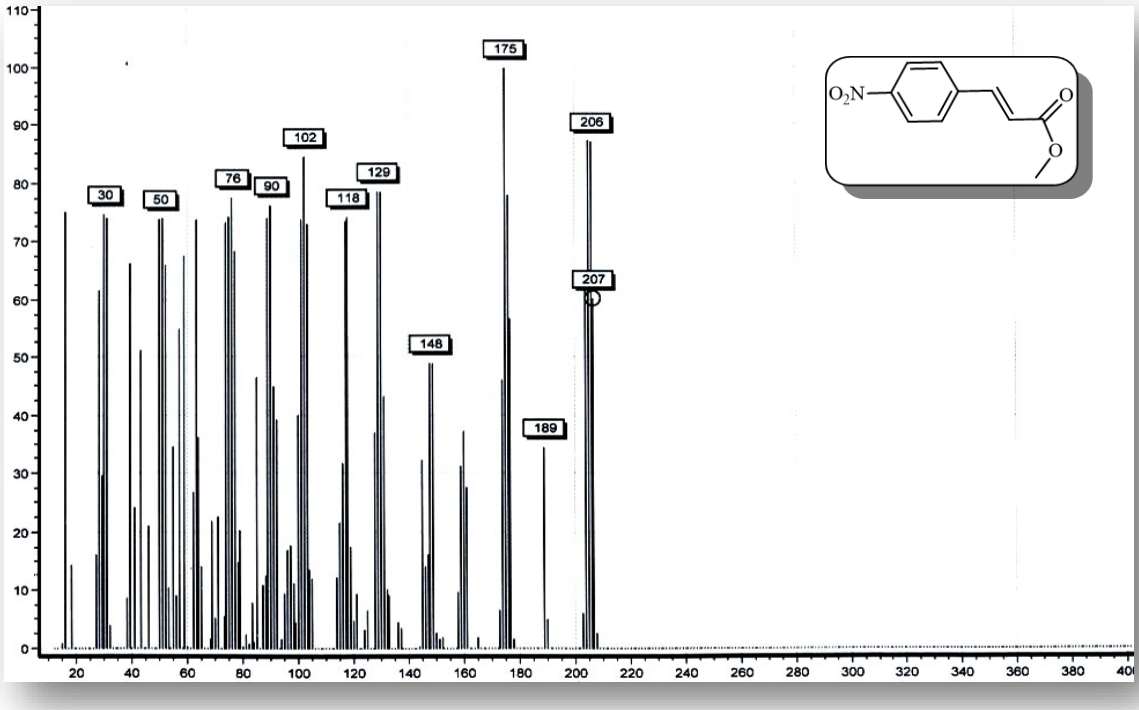

Fig. S20. Mass spectrum of (*E*)-Methyl 3-(4-nitrophenyl) acrylate (2d).

(*E*)-Butyl 3-(4-nitrophenyl)acrylate (**2f**) (0.216 g, 95%): white solid; mp 68-69 ºC (Lit.[5, 11, 14, 15] 67-69 ºC). δ_H (400 MHz, $CDCl_3$) 8.20 (d, *J* 8, 2H), 7.66 (d, *J* 16.1, 1H), 7.44 (d, *J* 8.7, 2H), 6.53 (d, *J* 16, 1H), 4.20 (t, *J* 6.7, 2H), 1.69-1.62 (m, 2H), 1.44-1.35 (m, 2H), 0.92 (t, *J* 7.2, 3H). δ_C (100 MHz, $CDCl_3$) 166.0, 148.3, 141.5, 140.5, 130.1, 128.6, 124.0, 122.5, 64.7, 30.6, 19.1, 13.6.

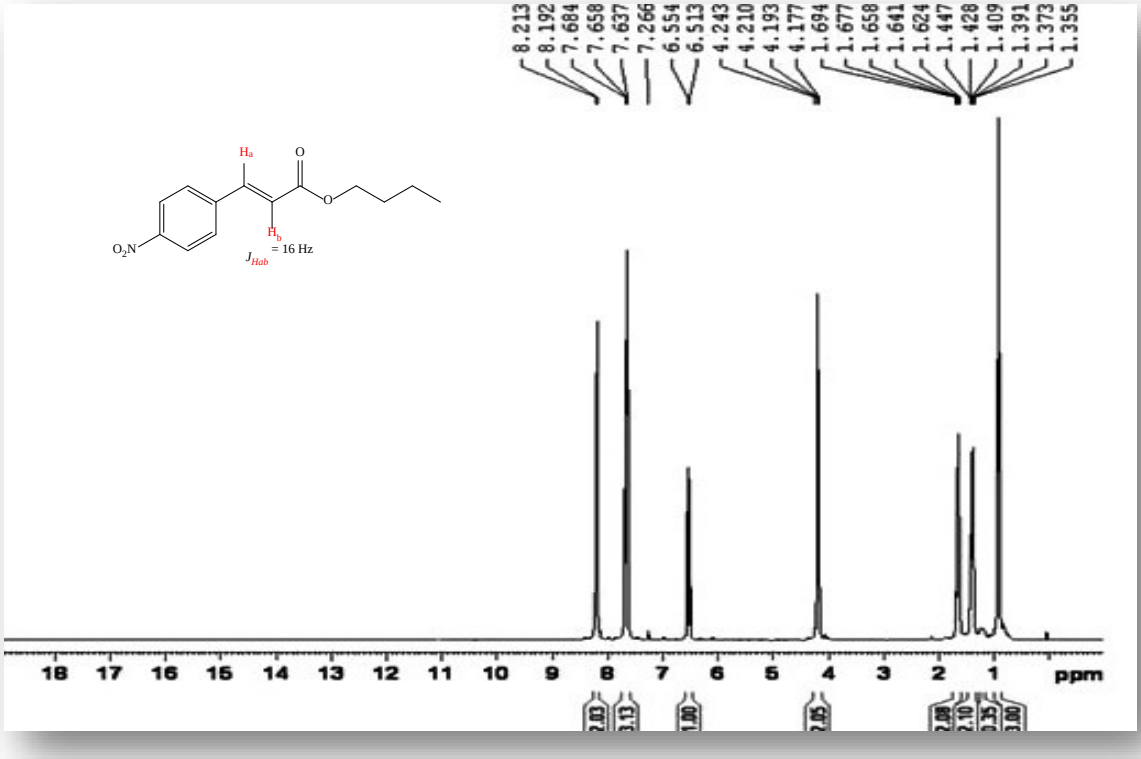

Fig. S21. ^{1}H NMR (400 MHz, $CDCl_3$) of (*E*)-Butyl 3-(4-nitrophenyl) acrylate (2f).

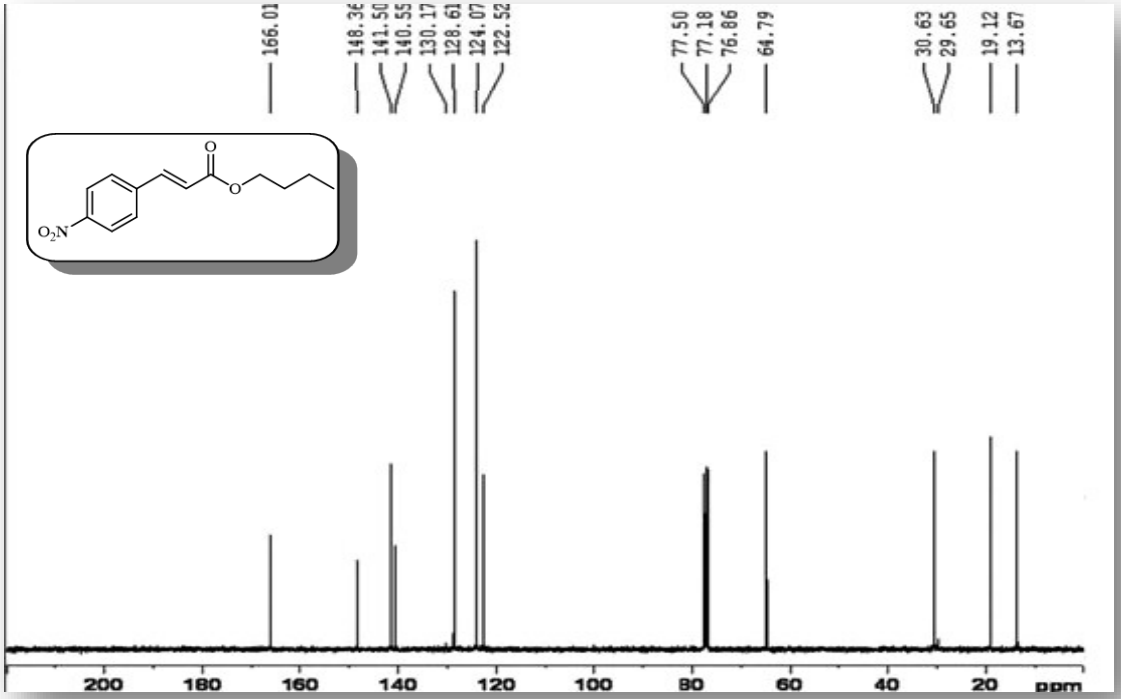

Fig. S22. ^{13}C NMR (100 MHz, $CDCl_3$) of (*E*)-Butyl 3-(4-nitrophenyl) acrylate (2f).

(*E*)-Methyl 3-(4-cyanophenyl)acrylate (**3d**) (0.243 g, 95%): white solid; mp 124-126 ºC (Lit.[6] 122-126 ºC). δ_H (300 MHz, $CDCl_3$) 7.69-7.61 (m, 4H), 7.58 (d, *J* 16.1, 1H), 6.51 (d, *J* 16, 1H), 3.82 (s, 3H). δ_C (75 MHz, $CDCl_3$) 166.6, 142.5, 138.8, 132.7, 128.5, 121.5, 118.4, 113.6, 52.0. *m/z* 187 (M^+, 55%), 186 (M-1H, 87), 155 (M-CH_6N, 103), 127 (M-$C_2H_4O_2$, 90), 101 (M-$C_4H_6O_2$, 78).

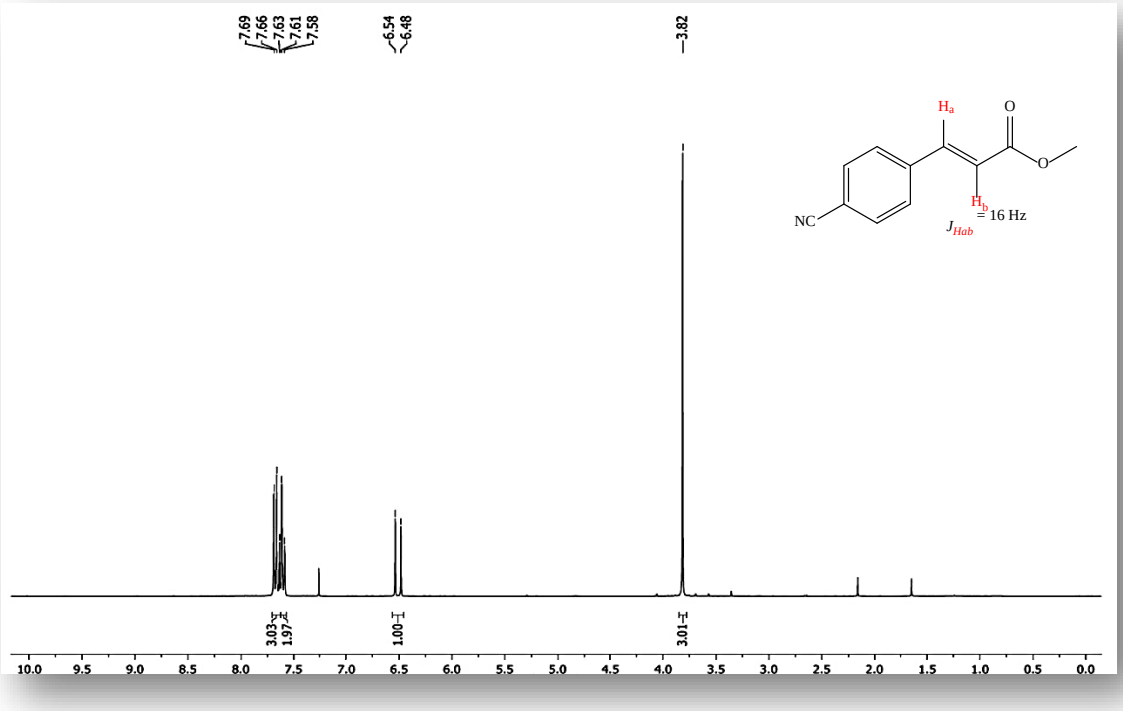

Fig. S23. ^{1}H NMR (300 MHz, $CDCl_3$) of (*E*)-Methyl 3-(4-cyanophenyl)acrylate (3d).

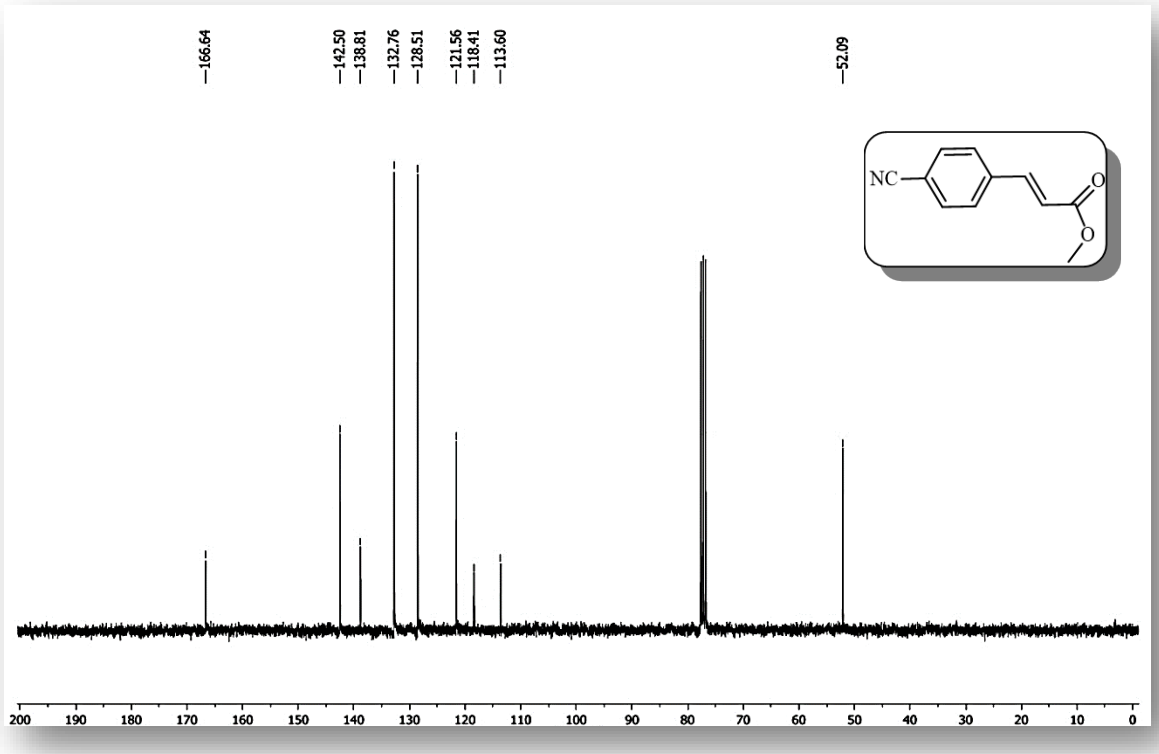

Fig. S24. ^{13}C NMR (75 MHz, $CDCl_3$) of (*E*)-Methyl 3-(4-cyanophenyl)acrylate (3d).

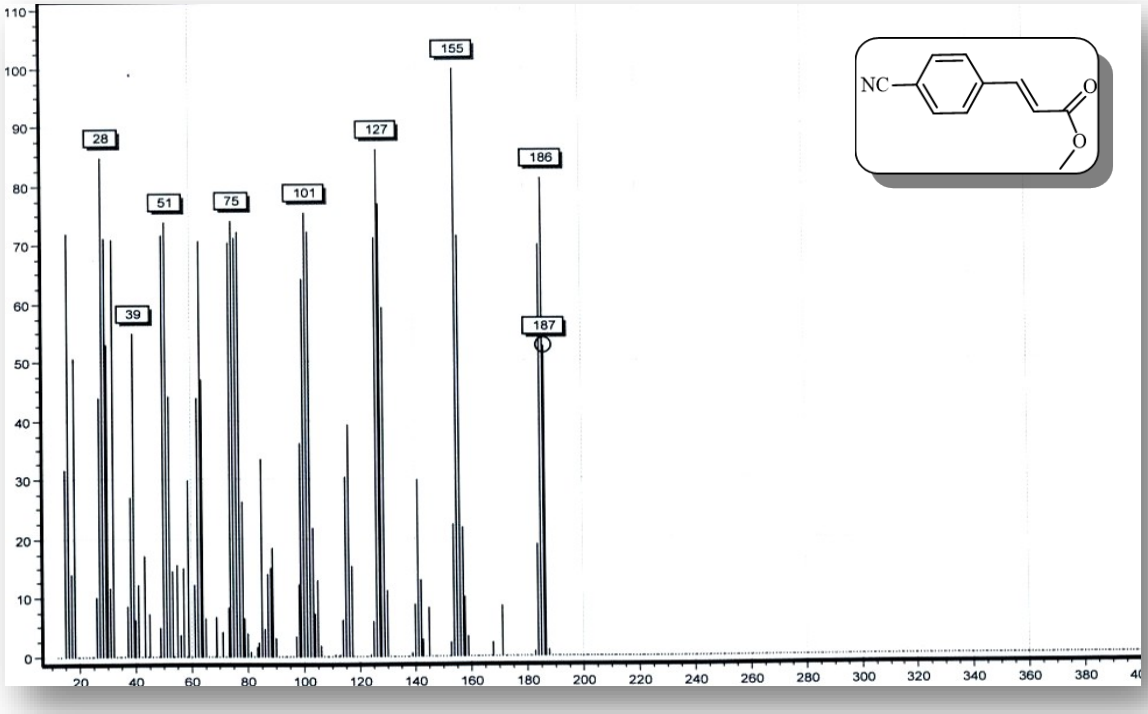

Fig. S25. Mass spectrum of (*E*)-Methyl 3-(4-cyanophenyl)acrylate (3d).

(*E*)-Methyl 3-(*p*-tolyl) acrylate (**4b**) (0.238 g, 85%): yellow solid; mp 56-57 ºC (Lit.[7, 12, 15] 55-57 ºC). δ_H (400 MHz, $CDCl_3$) 7.69 (d, *J* 16, 1H), 7.43 (d, *J* 8, 2H), 7.20 (d, *J* 8 2H), 6.41 (d, *J* 16, 1H), 3.81(s, 3H), 2.38 (s, 3H). δ_C (100 MHz, $CDCl_3$) 167.6, 144.8, 140.7, 131.6, 129.6, 128.0, 116.7, 51.6, 21.4. *m/z* 177 (M^+, 10 %), 175 (M-2H, 94), 160 (M-CH_4, 40), 144 (M-CH_4O, 100), 130 (M-C_3H_{10}, 38), 115 (M-C_2H_5O, 90), 102 (M-$C_3H_6O_2$, 52), 91 (M-$C_4H_5O_2$, 82).

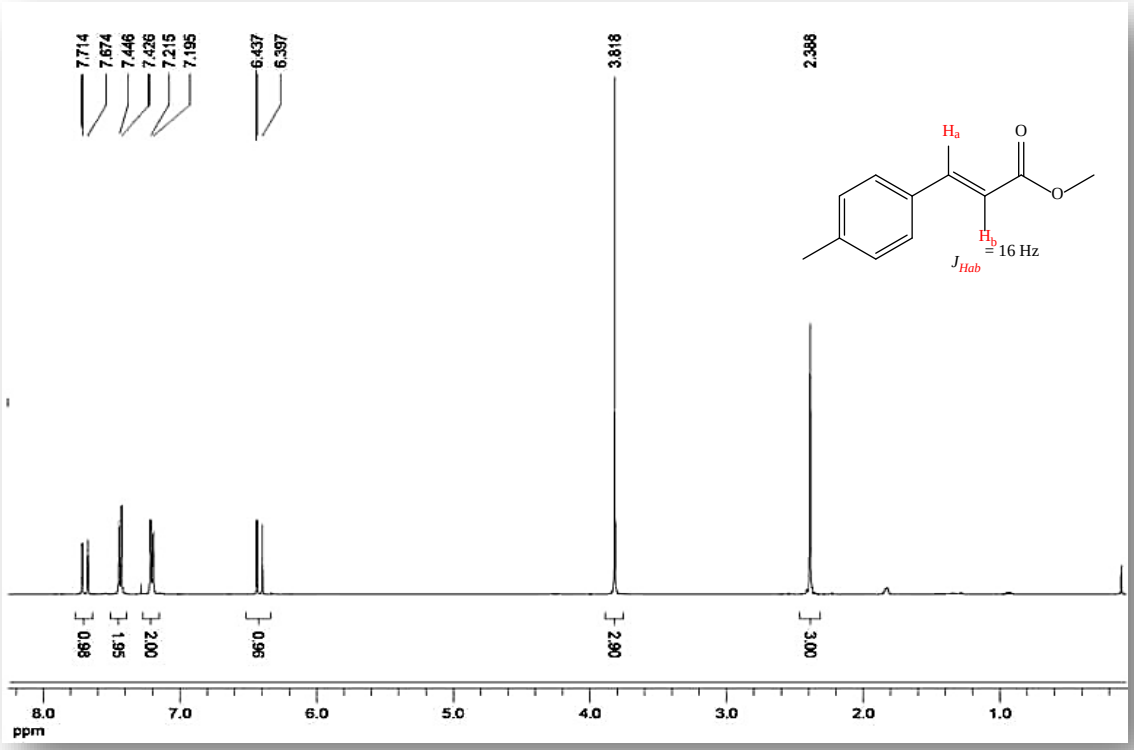

Fig. S26. ^{1}H NMR (400 MHz, $CDCl_3$) of (*E*)-Methyl 3-(*p*-tolyl) acrylate (4b).

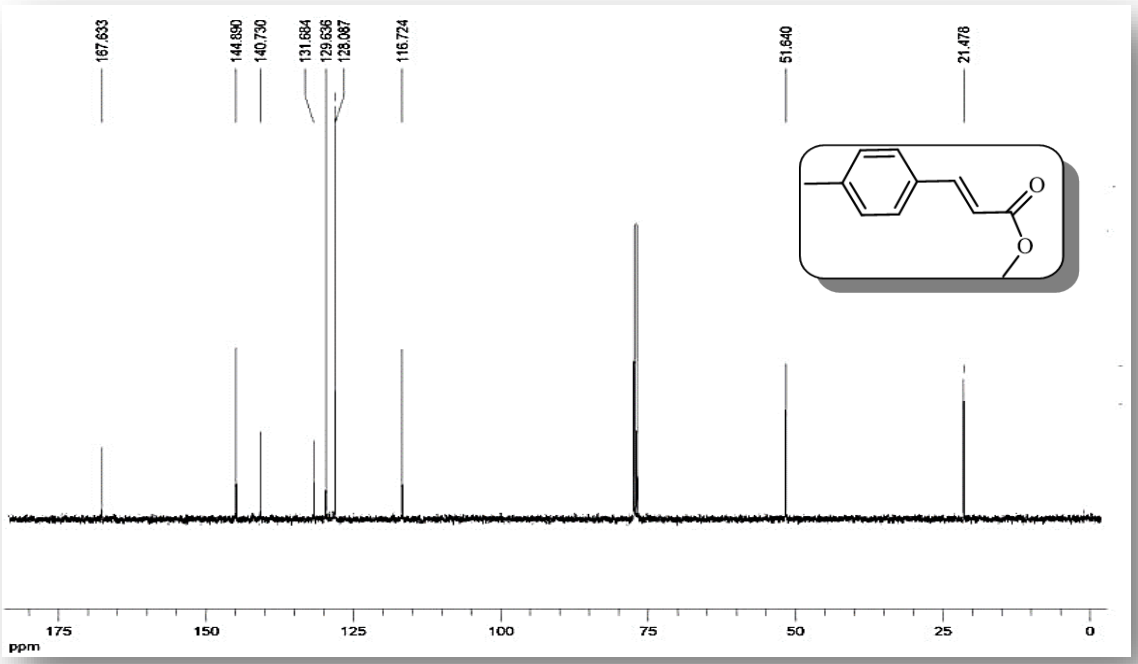

Fig. S27. ^{13}C NMR (100 MHz, $CDCl_3$) of (*E*)-Methyl 3-(*p*-tolyl) acrylate (4b).

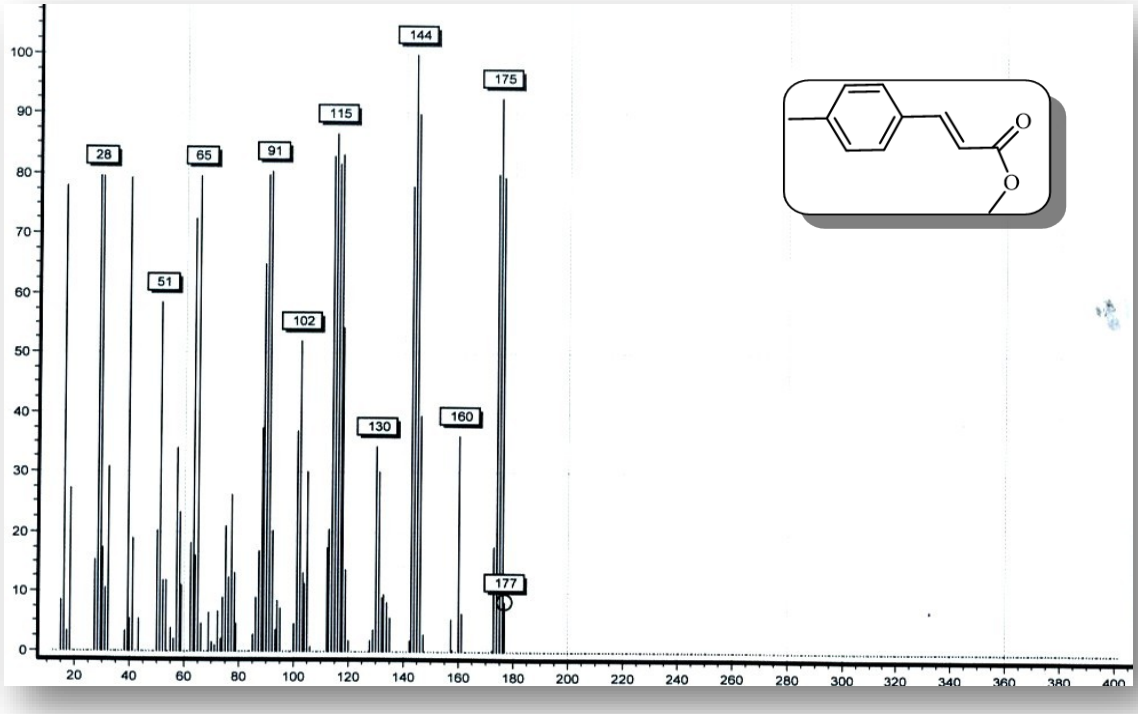

Fig. S28. Mass spectrum of (*E*)-Methyl 3-(*p*-tolyl) acrylate (4b).

(*E*)-Butyl 3-(*p*-tolyl)acrylate (**4d**) (0.244 g, 85%): oil; (Lit.[8, 11, 12, 14, 15]). δ_H (400 MHz, $CDCl_3$) 7.52 (d, *J* 16.1, 1H), 7.32-7.28 (m, 2H), 7.07-7.04 (m, 2H), 6.30 (d, *J* 16, 1H), 4.09 (t, *J* 5, 2H), 2.24 (s, 3H), 1.32-1.40 (m, 2H), 1.23-1.31 (m, 2H), 0.85 (t, *J* 7.4, 3H). δ_C (100 MHz, $CDCl_3$) 167.2, 144.5, 140.5, 131.7, 129.5, 128.0, 117.1, 64.2, 30.8, 21.4, 19.2, 13.7.

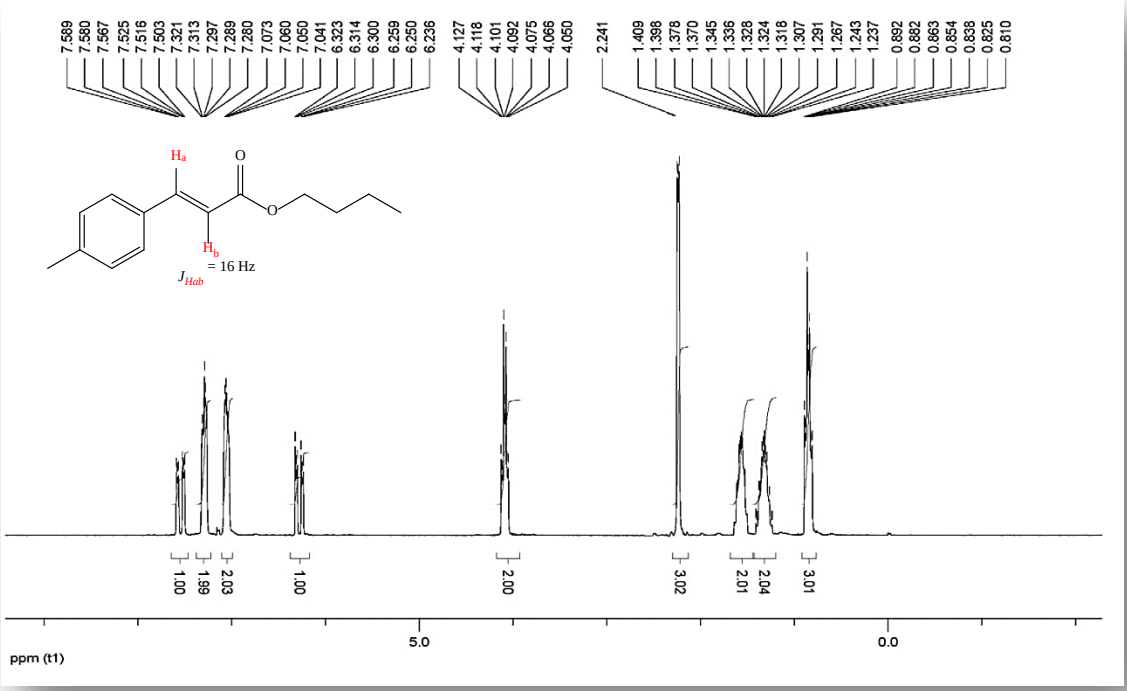

Fig. S29. ^{1}H NMR (400 MHz, $CDCl_3$) of (*E*)-Butyl 3-(*p*-tolyl) acrylate (4d).

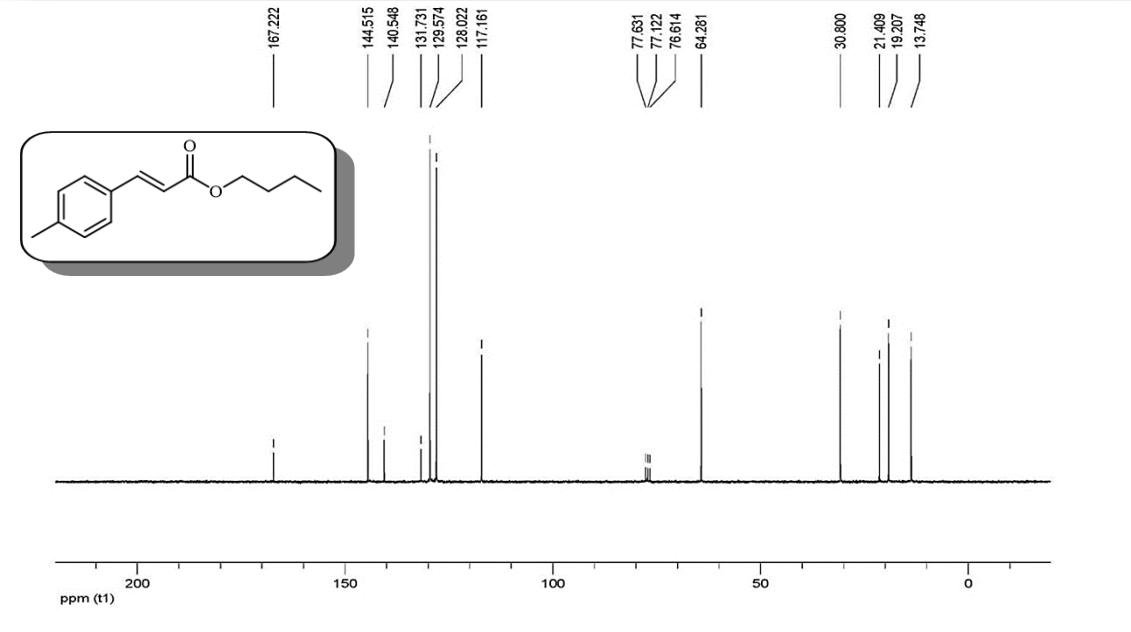

Fig. S30. ^{13}C NMR (100 MHz, $CDCl_3$) of (*E*)-Butyl 3-(*p*-tolyl) acrylate (4d).

(*E*)-Methyl 3-(4-methoxyphenyl)acrylate (**5b**) (0.261 g, 80%): yellow solid; mp 89-91 ºC (Lit.[6, 12] 88-91 ºC). δ_H (400 MHz, $CDCl_3$) 7.67 (d, *J* 16, 1H), 7.50-7.47 (m, 2H), 6.94-6.90 (m, 2H), 6.33 (d, *J* 16, 1H), 3.85 (s, 3H), 3.81 (s, 3H). δ_C (100 MHz, $CDCl_3$) 167.8, 161.4, 144.6, 129.8, 127.2, 115.3, 114.4, 55.4, 51.6. *m/z* 192 (M^+, 95), 191 (M-1H, 100), 160 (M-CH_4O, 100), 133 (M-$C_2H_3O_2$, 98), 118 (M-$C_3H_6O_2$, 37), 89 (M-C_7H_3O, 49).

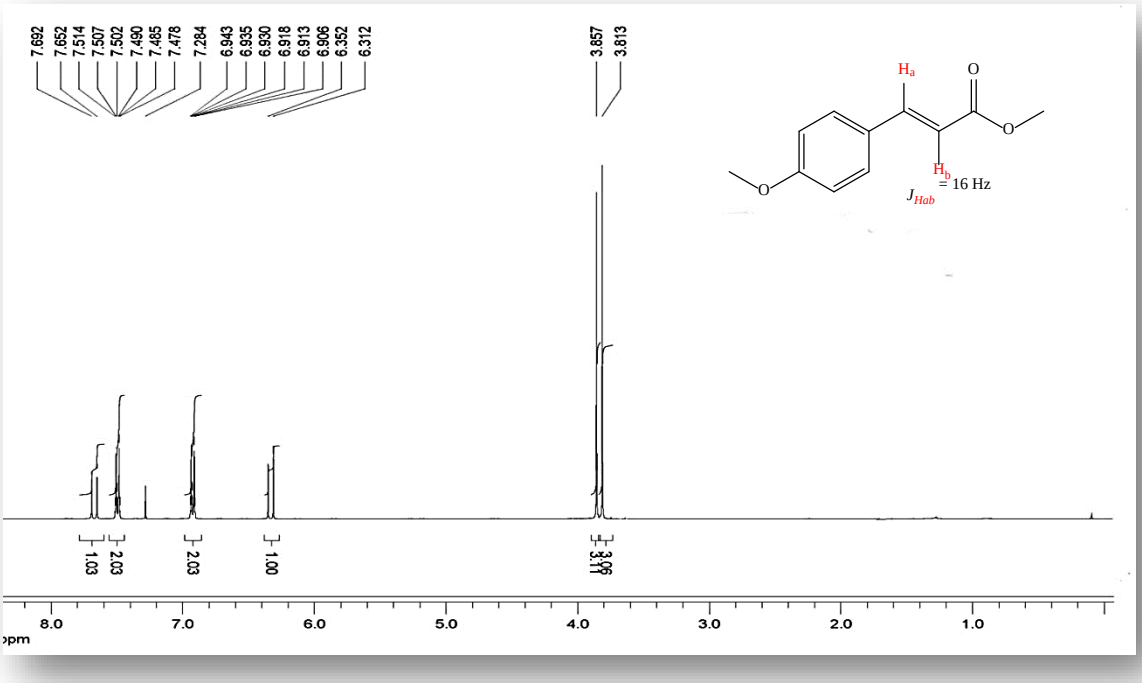

Fig. S31. ^{1}H NMR (400 MHz, $CDCl_3$) of (*E*)-Methyl 3-(4-methoxyphenyl)acrylate (5b).

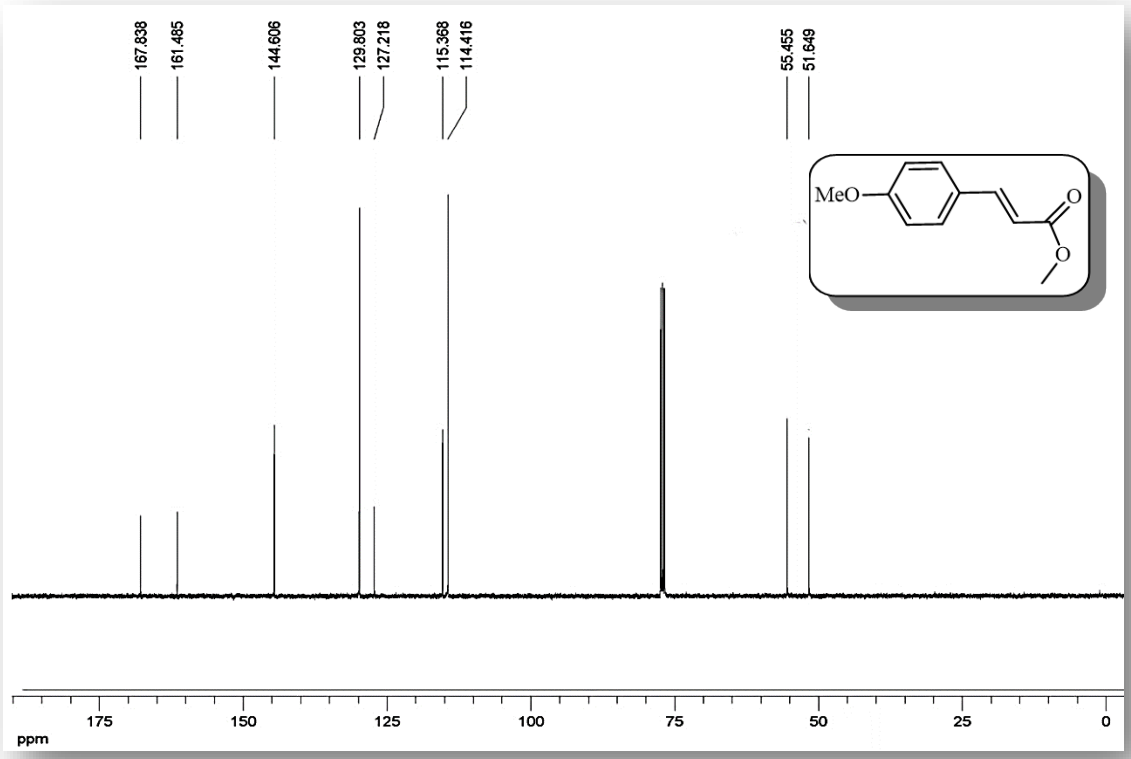

Fig. S32. ^{13}C NMR (100 MHz, $CDCl_3$) of (*E*)-Methyl 3-(4-methoxyphenyl)acrylate (5b).

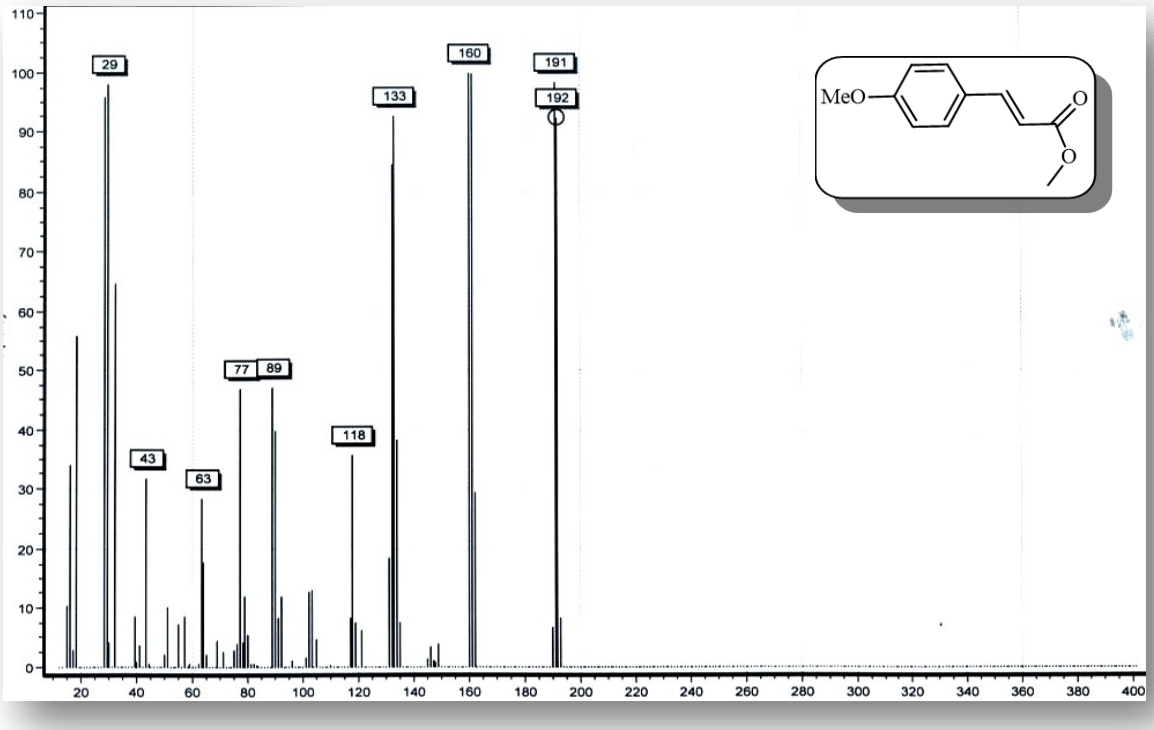

Fig. S33. Mass spectrum of (*E*)-Methyl 3-(4-methoxyphenyl)acrylate (5b).

(*E*)-Butyl 3-(4-methoxyphenyl)acrylate (**5d**) (0.176 g, 75%): white solid; mp 90-92 ºC (Lit.[9, 11, 12, 14, 15] 90-92 ºC). δ_H (400 MHz, $CDCl_3$) 7.67 (d, *J* 16, 1H), 7.39 (d, *J* 4.2, 2H), 6.81 (d, *J* 4.8, 2H), 6.24 (d, *J* 16, 1H), 4.13 (t, *J* 7, 2H), 3.72 (s, 3H), 1.60-1.62 (m, 2H), 1.35-1.40 (m, 2H), 0.91 (t, *J* 7, 3H). δ_C (100 MHz, $CDCl_3$) 167.8, 161.4, 144.6, 129.8, 127.2, 115.3, 114.4, 55.4, 51.6. *m/z* 234 (M^+, 5 %), 232 (M-2H, 97), 190 (M-C_2H_5O, 15), 177 (M-C_4H_9, 100), 160 (M-$C_4H_{10}O$, 100), 133 (M-$C_5H_9O_2$, 92), 120 (M-$C_6H_{10}O_2$, 80).

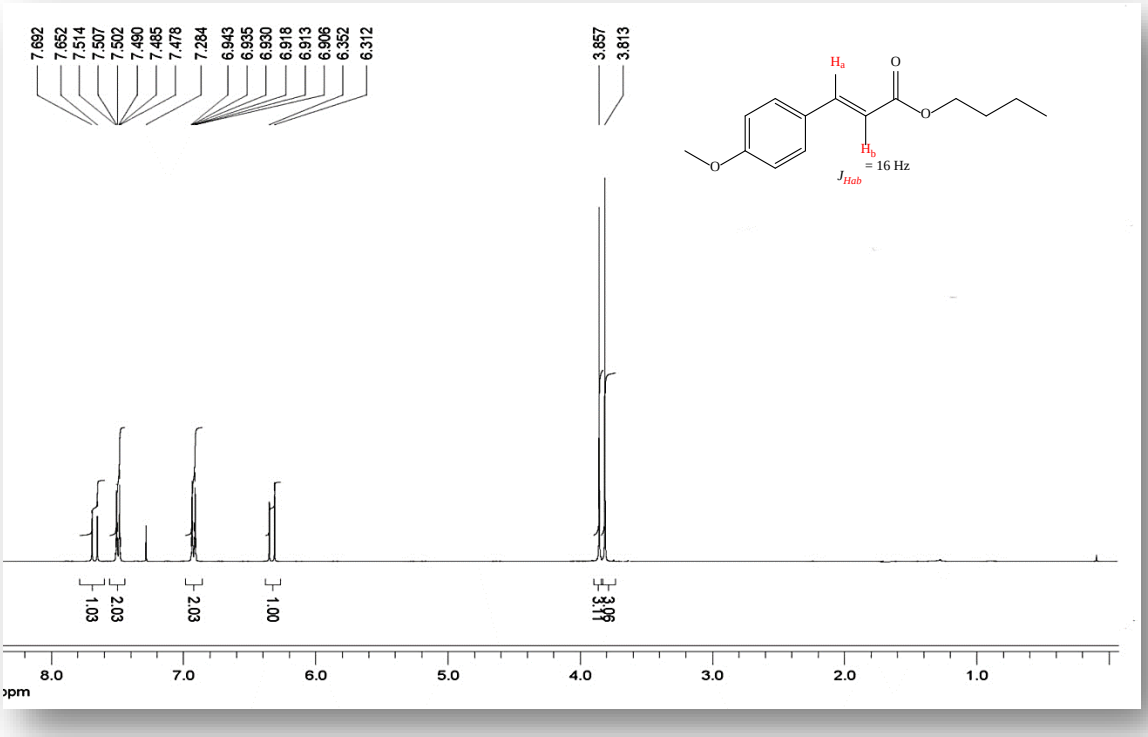

Fig. S34. ^{1}H NMR (400 MHz, $CDCl_3$) of (*E*)-Butyl 3-(4-methoxyphenyl) acrylate (5d).

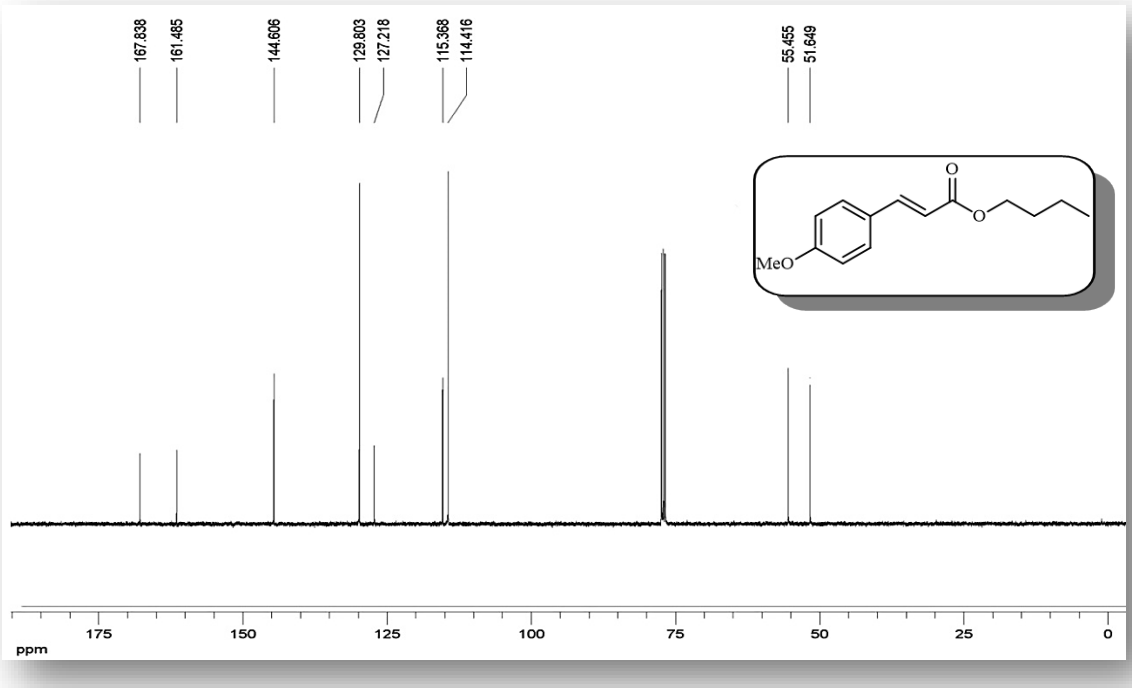

Fig. S35. ^{13}C NMR (100 MHz, $CDCl_3$) of (*E*)-Butyl 3-(4-methoxyphenyl) acrylate (5d).

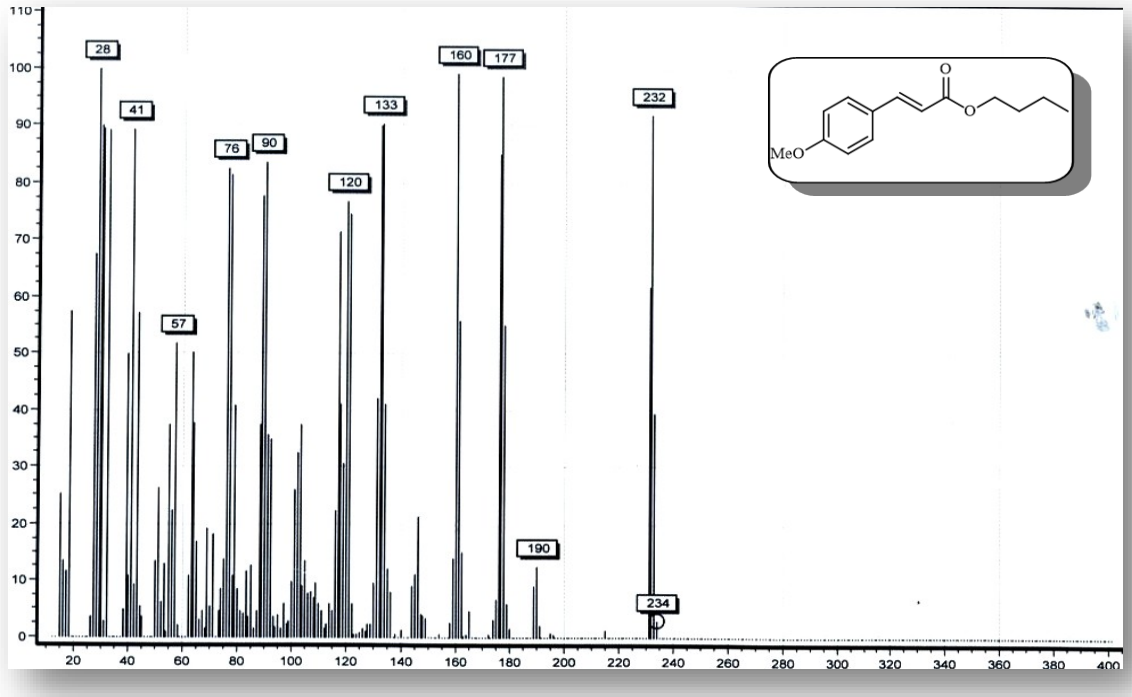

Fig. S36. Mass spectrum of (*E*)-Butyl 3-(4-methoxyphenyl) acrylate (5d).

(*E*)-Methyl cinnamate (**6d**) (0.254 g, 90%): white solid; mp 36-37 ºC (Lit.[4, 12, 15] 35-37 ºC). δ_H (400 MHz, $CDCl_3$) 7.60 (d, *J* 16, 1H), 7.43-7.41 (m, 2H), 7.29-7.27 (m, 3H), 6.34 (d, *J* 16, 1H), 3.70 (s, 3H). δ_C (100 MHz, $CDCl_3$) 166.9, 144.3, 133.9, 129.8, 128.4, 127.6, 117.3, 51.2. *m/z* 162 (M^+, 62), 161 (M-1H, 89), 131 (M-CH_3O, 101), 117 (M-C_3H_9, 34), 103 (M-$C_2H_3O_2$, 92), 91 (M-$C_3H_3O_2$, 58).

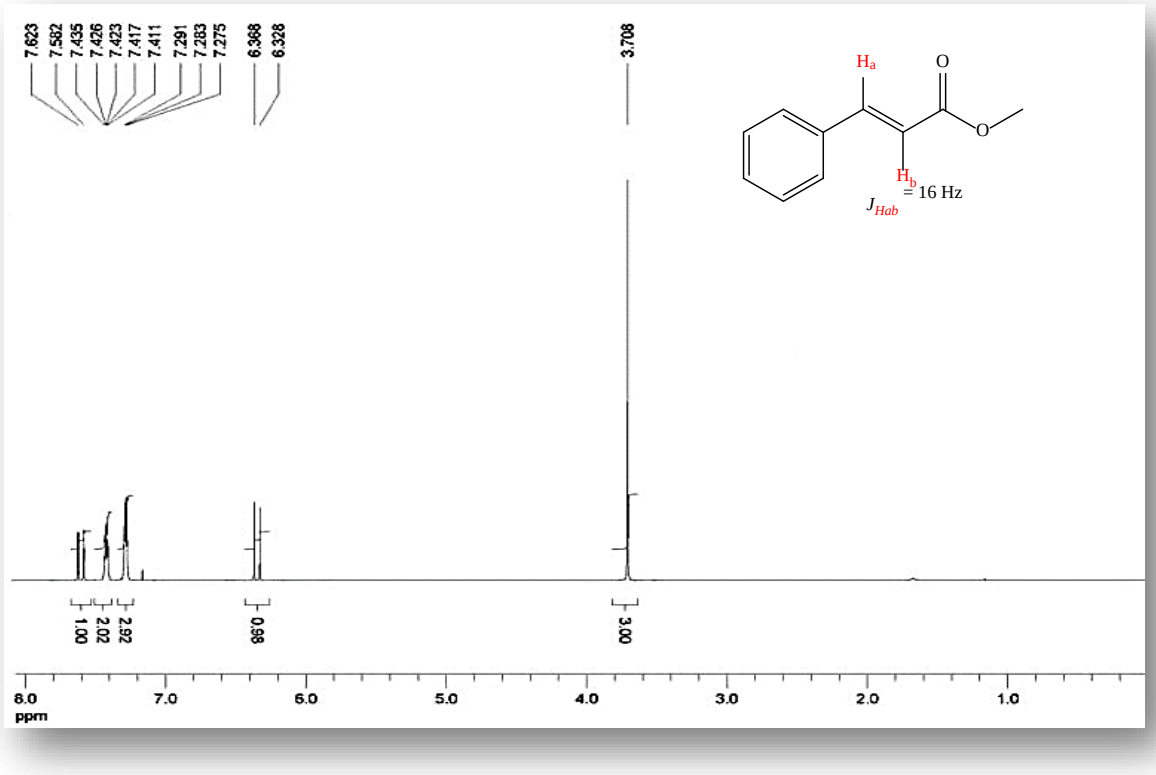

Fig. S37. ^{1}H NMR (400 MHz, $CDCl_3$) of (*E*)-Methyl cinnamate (6d).

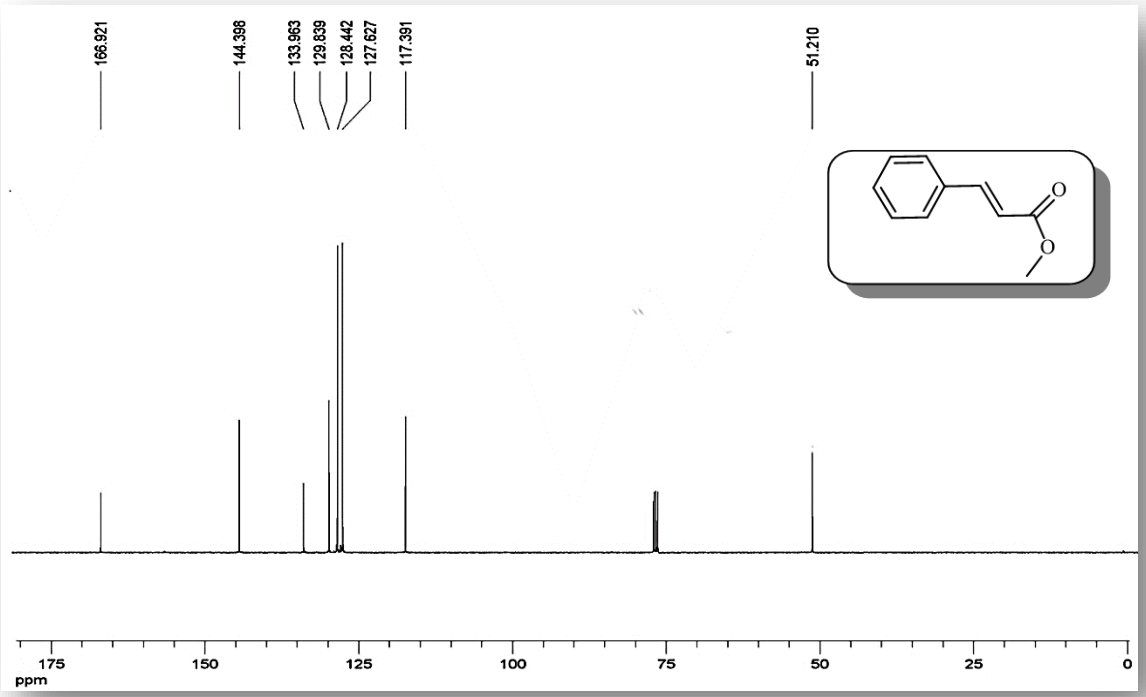

Fig. S38. ^{13}C NMR (100 MHz, $CDCl_3$) of (*E*)-Methyl cinnamate (6d).

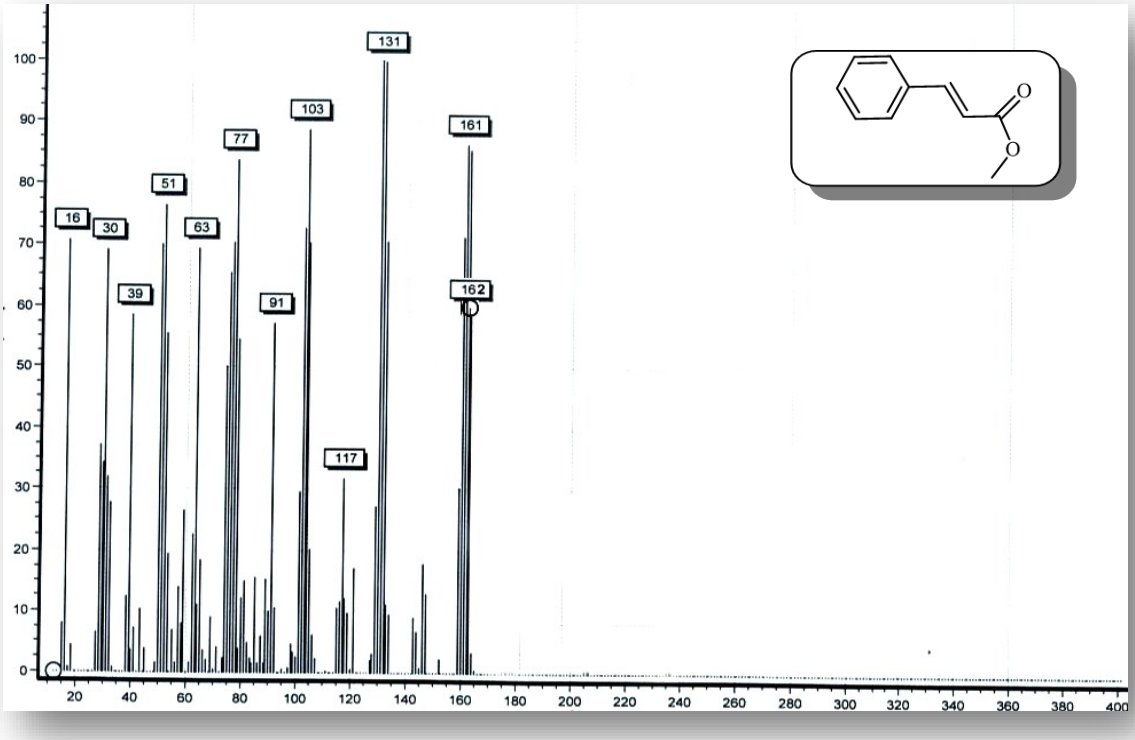

Fig. S39. Mass spectrum of (*E*)-Methyl cinnamate (6d).

References

[1] S. Rostamnia, H. Alamgholiloo, X. Liu, *J. Colloid Interface Sci.* **2016**, 469, 310.

[2] D. H. Ortgies, A. Barthelme, S. Aly, B. Desharnais, S. Rioux, P. Forgione, *Synthesis* **2013**, 45, 694.

[3] M. Amini, H. Etemadi, *Chem. Pap.* **2013**, 67, 759.

[4] K. S. Nalivela, M. Tilley, M. A. McGuire, M. G. Organ, *Chem. Eur. J.* **2014**, 20, 6603.

[5] X. Zhou, J. Luo, J. Liu, S. Peng, G. J. Deng, *Org. Lett.* **2011**, 13, 1432.

[6] B. Schmidt, R. Berger, *Adv. Synth. Catal.* **2013**, 355, 463.

[7] B. R. Ambler, R. A. Altman, *Org. Lett.* **2013**, 15, 5578.

[8] P. Cyr, S. T. Deng, J. M. Hawkins, K. E. Price, *Org. Lett.* **2013**, 15, 4342.

[9] F. Ebrahimzadeh, B. Tamami, *Phosphorus Sulfur Silicon Relat. Elem.* **2015**, 190, 144.

[10] A. N. Chinchole1, A. V. Dubey1, A. V. Kumar, *Catal. Lett.* **2019**, 149, 1224.

[11] A. R. Sardarian, M. Kazemnejadi, M. Esmaeilpour, *Dalton Trans.* **2019**, 48, 3132.

[12] S. K. Bhat, J. D. Prasad, M. S. Hegde, *J. Chem. Sci.* **2019**, 131, 20.

[13] A. Takallou, A. Habibi, A. Z. Halimehjani, S. Balalaie, *J. Organomet. Chem.* **2019**, 888, 24.

[14] P. Wang, H. Liu, M. Liu, R. Li, J. Ma, *New J. Chem.* **2014**, 38, 1138.

[15] S. Sobhani, M. S. Ghasemzadeh, M. Honarmand, F. Zarifi, *RSC Adv.* **2014**, 4, 44166.